Chinese Journal of Mechanical Engineering

ORIGINAL ARTICLE

Open Access

Evaluation on Configuration Stiffness of Overconstrained 2R1T Parallel Mechanisms

Xuejian Ma[1], Zhenghe Xu[1], Yundou Xu[1,2*], Yu Wang[1], Jiantao Yao[1,2] and Yongsheng Zhao[1,2*]

Abstract

Currently, two rotations and one translation (2R1T) three-degree-of-freedom (DOF) parallel mechanisms (PMs) are widely applied in five-DOF hybrid machining robots. However, there is a lack of an effective method to evaluate the configuration stiffness of mechanisms during the mechanism design stage. It is a challenge to select appropriate 2R1T PMs with excellent stiffness performance during the design stage. Considering the operational status of 2R1T PMs, the bending and torsional stiffness are considered as indices to evaluate PMs' configuration stiffness. Subsequently, a specific method is proposed to calculate these stiffness indices. Initially, the various types of structural and driving stiffness for each branch are assessed and their specific values defined. Subsequently, a rigid-flexible coupled force model for the over-constrained 2R1T PM is established, and the proposed evaluation method is used to analyze the configuration stiffness of the five 2R1T PMs in the entire workspace. Finally, the driving force and constraint force of each branch in the whole working space are calculated to further elucidate the stiffness evaluating results by using the proposed method above. The obtained results demonstrate that the bending and torsional stiffness of the 2RPU/UPR/RPR mechanism along the *x* and *y*-directions are larger than the other four mechanisms.

Keywords Parallel mechanism, Stiffness, Over-constrained, Three degrees of freedom

1 Introduction

Studies show that numerous parallel mechanisms (PMs) for diverse applications have been proposed so far. Among different types of lower-mobility PMs, the two-rotational-degrees-of-freedom and one-translational-degree-of-freedom (2R1T) PM are the most important ones. It should be indicated that 3RPS PM [1] is a typical 2R1T-PM. In 1983, Hunt [1] proposed the 3RPS PM that widely attracted many researchers. In this regard, investigations have been carried out to study 2R1T PM from different aspects, including synthesis, kinematics, parasitic motion, singularity analysis, and dimension synthesis [2–10]. Recently, modified 2R1T PMs have been proposed, which have been applied widely in diverse fields such as A3 machine tool head based on the 3RPS PM [2, 4, 11], Sprint Z3 tool head based on the 3PRS PM [12, 13], Tricept [14], TriVariant [15], five-DOF parallel-serial manipulators based on 3UPS-UP and 2UPS-UP PMs, and Exechon five-axis machining center based on the 2UPR-SPR PM [16, 17], which are typical applications of the 2R1T-PMs. It is worth noting that R, P, S, and U denote revolute, prismatic, spherical, and universal joints, respectively.

In the type synthesis of the 2R1T PMs, different aspects, including over-constraints [18–20], symmetry [5, 21], decoupled motions [22–25], accompanying motions [26, 27], continuous axes [28–31] and a number of kinematic joints [32] etc., have been taken into account. However, for the designed PM-based equipment, stiffness is an important index that affects the device performance.

*Correspondence:
Yundou Xu
ydxu@ysu.edu.cn
Yongsheng Zhao
yszhao@ysu.edu.cn; caffeezhang@hotmail.com
[1] Parallel Robot and Mechatronic System Laboratory of Hebei Province, Yanshan University, Qinhuangdao 066004, China
[2] Key Laboratory of Advanced Forging and Stamping Technology and Science of Ministry of National Education, Yanshan University, Qinhuangdao 066004, China

The configuration stiffness of a mechanism refers to the end-effector displacement caused by the deformation of its parts under the action of external forces, where the structure shape and size are not determined yet, which plays a decisive role in the motion accuracy of the mechanism. However, during the configuration design of the parallel robot mechanism, no effective method has yet been proposed to evaluate the configuration stiffness of the robot.

Several approaches can be applied to calculate the stiffness matrix. These approaches mainly differ in the model assumptions and computational techniques [33–36]. Reviewing the literature indicates that the finite element method (FEM) [37, 38], matrix structure method (MSM) [39], virtual joints method (JVM) [40–42], and screw-based method (SBM) [43–47] are the most commonly used approaches in this regard. Generally, the finite element method is applied at the final design stage for the verification and component dimensioning. Moreover, the matrix structure method needs tedious calculations. The JVM and SBM methods have a clear physical interpretation and can accurately reflect the correlation between the stiffness of PMs and the stiffness along the axes of the constraint wrenches. In the latter two methods, actual stiffness models of actuation units, transmissions, passive joints, and connecting links are considered to establish the overall stiffness matrix of the robot [48, 49]. The singular value decomposition can be carried out on the stiffness matrix to get the direction of the maximum and the minimum stiffness and obtain the maximum and minimum deformations accordingly [50–52]. However, the stiffness matrix model involves the robot parts' specific structural shape and size, while the modeling process is quite complicated. Meanwhile, this method does not guarantee the same size for different mechanisms. Since the stiffness matrix has different dimensions, it is impossible to judge the maximum and minimum stiffness accurately. Hu and Huang [53] obtained the stiffness model of a 2RPU-UPR (U = universal joint, P = prismatic joint, R = revolute joint) over-constrained parallel manipulators. Yang and Li [54] propose a unified method for the elastostatic stiffness modeling of over-constrained parallel manipulators. Ding et al. [55] analyzed the accuracy of an over-constrained Stewart platform with actuation stiffness. Cao et al. [56, 57] obtained the stiffness model of over-constrained parallel manipulators by using an energy method with less than 3% accuracy loss only under an external wrench. Cao et al. [58] extended the approach by considering the weights of the links in which the weight of each limb is distributed between the mobile platform frame and the base. Finally, Klimchik et al. [59] derived the stiffness model of NAVARO II, which is a novel variable actuation mechanism based on active and passive pantographs. The connection method of multiple closed-loop chains is illustrated for an external wrench on the mobile platform via SMA; however, the dimensions of the matrices to be computed were relatively high. The fundamentals of the SMA methodology are given in Ref. [60].

A variety of stiffness evaluation indexes of parallel mechanisms have been proposed, such as eigenvalue index [61, 62], determinant value index [63], trace of matrix [63], Weighted index of trace [64], main diagonal index of stiffness matrix [65], virtual work index [61]. However, the above stiffness indexes are obtained based on the overall stiffness matrix of the mechanism, these indexes do not consider the influence of structural composition on the mechanism stiffness in all directions. And this cannot reflect the weaker direction of the PM stiffness in the mechanism design stage. From the structural composition point of view, it can be concluded that the PM has weak stiffness in bending and torsional direction, while the tensile and compressive stiffness is relatively strong, because the axial load is generally borne by driving forces of all branches together, but it can be seen as a cantilever system when the bending forces and torsional torques are imposed. For this reason, this study proposes bending and torsional stiffness indexes of parallel mechanisms considering the structural constraints, and compares the bending and torsional stiffness of several 2R1T parallel mechanisms to select the preferred one with good stiffness performance.

As the extension length of the working arm becomes longer, the bending and torsional stiffness gradually decrease, and the imposed load on the branch and part of the branch are entirely different. This phenomenon mainly originates from different compositions and distributions of the constraint forces/couples under the action of the external load at the end. For example, for the 2UPR-SPR PM [66] that constitutes the Exechon five-axis hybrid machining center, all three driving branches bear the external load of the constrained space and the driving space simultaneously. However, for the 3UPS-UP PM [67] that constitutes the Tricept five-axis hybrid robot, the constraint branch UP completely tolerates the external load in the constrained space. Meanwhile, different robots may have different structural branches, actuation unit stiffness, transmission devices, and connecting links. This issue is significantly more pronounced for the stiffness of the driving unit and transmission device along the non-main direction so that the stiffness performance of different mechanisms may be different. Therefore, evaluating the configuration stiffness considering the structural constraints of the parallel mechanism, lacks simple evaluation criteria. Configuration stiffness means the mechanism stiffness during the design stage

where the structure shape and size are not determined yet. Accordingly, it is an enormous challenge to select the best mechanism with optimal stiffness performance during the design stage.

In the present study, the PMs' bending and torsional stiffness indices will be defined. Then these indices will be applied to a five-axis hybrid robot in an engineering case study. For the studied case, values of the driving and structural stiffness of each part in the branch that affect the overall stiffness of the mechanism will be directly defined. Then the global stiffness of the parallel mechanism can be obtained, and all the bending deformation and torsional deformation are obtained based on the over-constrained PM's force analysis. What's next, all the driving and constraint forces/couples are obtained, which are used to explain the reasons for the configuration stiffness evaluating results. Finally, through Ansys software, the stiffness of five parallel mechanisms is simulated to verify the correctness of the stiffness evaluating indices and methods. This article is expected to provide a new and simple way to evaluate the stiffness performance of PMs during the mechanism design stage.

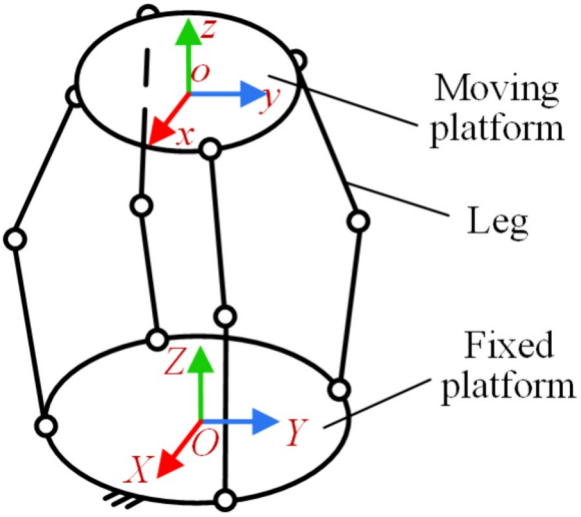

Figure 1 Schematic diagram of the parallel mechanism

2 Stiffness Evaluation Index and Evaluation Criterion

In the present study, the bending stiffness of PMs is defined as the capability of the mechanism to resist the bending deformation, specifically under the action of a lateral unit force on the moving platform. Under the action of a unit lateral force on the moving platform, the linear deformation of the parallel mechanism based on the global stiffness model is solved according to the defined branch stiffness. The average linear deformations of the mechanism indicate values of the bending stiffness of PMs.

The bending stiffness of the mechanism can be divided into the stiffness in the lateral x and y-axis, respectively. Figure 1 shows that at the origin of the moving coordinate system at the end of the mechanism, the lateral unit force is exerted along the x and y-direction, respectively.

Furthermore, torsional stiffness is defined as the capability of the mechanism to resist torsional deformation, specifically under the action of a unit torque along the normal line of the moving platform on the moving platform. Under the action of a unit torque along the moving platform's normal direction, the parallel mechanism's angular deformation based on the global stiffness model is solved according to the defined branch stiffness. Similarly, the average of angular deformations of the parallel mechanism can be calculated, indicating the values of PMs' torsional stiffness.

Based on the above definition, the main factors affecting the bending and torsional stiffness of the 2R1T PM are the stiffness of each branch. Considering the actual PM-based designed equipment, the branch stiffness is affected by the structural stiffness of the links, joints, and the stiffness of driving units. And based on the engineering experience, considering the strength and weakness of the stiffness of these branch parts, different values of the stiffness are defined to get the linear and angular deformations of the mechanism so that the PM with relatively better stiffness performance can be selected. For example, the bending and torsional stiffness of the linear driving unit is relatively weak among those structures mentioned above in each branch, so their defined values should be smaller.

In order to compare the stiffness performance of the PMs qualitatively, the global bending and torsional performance indices can be mathematically expressed as follows:

$$\Gamma_{\omega} = \frac{\int_w \omega_i \mathrm{d}w}{\int_w \mathrm{d}w}, \tag{1}$$

$$\Gamma_{\varphi} = \frac{\int_w \varphi_i \mathrm{d}w}{\int_w \mathrm{d}w}, \tag{2}$$

where Γ_{ω} and Γ_{ϕ} are the bending and torsional stiffness performance indices, respectively. Meanwhile, Γ_{ω} can be divided into Γ_{ω}^{x} and Γ_{ω}^{y} along in x- and y-directions, respectively. Moreover, ω_i and ϕ_i denote linear deformation and torsional angle deformation values at the sample point i, respectively. i is the number of samples, and w denotes the workspace.

3 Research Object

In the present study, the over-constrained 2R1T parallel mechanism 2RPU/UPR (proposed by Li et al. [29]), 2RPU/UPR/RPR, 3UPS/UP, 2UPU/SP, and 2UPR/SPR are considered as the research object. These mechanisms are schematically presented in Figure 2. It is worth noting that there are two PMs containing three branches and two PMs containing four branches, and the structure of the PMs with the same number of branches are different, thus the constraint wrenches provided by the branches for these five mechanisms are all different. Moreover, these mechanisms consist of the parallel part of four 5-DOF hybrid robots [32, 68–70] and the classic hybrid robot Exechon [66]. And this section is intended to analyze and compare the configuration stiffness of PMs of these five hybrid robots.

The driving and constraint wrenches exerted to the moving platform by each branch are initially analysed. For the 2RPU/UPR PM, the exerted driving and constraint wrenches to the moving platform are $\$_{11}^r$, $\$_{12}^r$, $\$_1^a$, $\$_{21}^r$, $\$_{22}^r$, $\$_2^a$, $\$_{31}^r$, $\$_{32}^r$, and $\$_3^a$. Moreover, the driving and constraint wrenches for the 2RPU/UPR/RPR PM are $\$_{11}^r$, $\$_{12}^r$, $\$_1^a$, $\$_{21}^r$, $\$_{22}^r$, $\$_2^a$, $\$_{31}^r$, $\$_{32}^r$, $\$_3^a$, $\$_{41}^r$, $\$_{42}^r$, and $\$_{43}^r$. For the 3UPS/UP PM, the driving and constraint wrenches are $\$_1^a$, $\$_2^a$, $\$_3^a$, $\$_{41}^r$, $\$_{42}^r$, and $\$_{43}^r$. For the 2UPR/SPR PM, the driving and constraint wrenches are $\$_{11}^r$, $\$_{12}^r$, $\$_1^a$, $\$_{21}^r$, $\$_{22}^r$, $\$_2^a$, $\$_{31}^r$, and $\$_3^a$. Finally, the driving and constraint wrenches of the moving platform for the 2UPU/SP PM are $\$_{11}^r$, $\$_{12}^r$, $\$_1^a$, $\$_{21}^r$, $\$_{22}^r$, $\$_2^a$, $\$_{31}^r$, $\$_{32}^r$, and $\$_3^a$. As shown in the Figure 2, the black arrows indicate the driving wrench while the red arrows indicate the constraint wrench.

Suppose that each branch's upper and lower connecting links are cylindrical rods with structural parameters given in Table 1, where μ is Poisson's ratio, $2a$, and $2b$ are the length of the triangular base of the moving and fixed platform, respectively. Moreover, ϕ is the angle between two hypotenuses of a fixed platform, h is the initial distance between moving and fixed platforms, l_{i1} (i=1,2,3,4) is the initial length of the lower connecting link of each branch, d_{i1} and d_{i2} are the cross-section diameters of the upper and lower connecting links, respectively. And the diameter of P joint is d_p, length is l_p.

Let α and β be angled rotating around the axes of two rotational DOFs r_1 and r_2, with initial values of α=β=0°. Then the length of each branch (i.e., l_1, l_2, l_3, and l_4) can be determined through the inverse position solution of the parallel mechanism.

4 Configuration Stiffness Analysis and Comparison

4.1 Configuration Stiffness Analysis

The five 2R1T PMs have common features, including linear drive unit, prismatic joint, revolute joint and rod. Based on the experience of structural design of the robots, for example, the flexural stiffness of the driving structure should be lower, since the transmission device has weak stiffness in the lateral direction. Consequently, simplified models of five PMs with the same size are designed, based on which the stiffness values of each part are defined. Table 2 gives the specific values of four kinds of branch stiffness affecting the bending and torsional stiffness of the mechanisms.

The given stiffness of the rod includes axial stiffness, flexural stiffness and torsional stiffness. Moreover, structural stiffness of the R joint includes torsional stiffness, tension and compression stiffness. Finally, the structural stiffness of the P joint includes flexural stiffness and torsional stiffness. The axial stiffness of the P joint refers to the capability of the driving device, which is along the axial direction of driving force.

The compliance matrices of revolute joints, prismatic, and each branch's lower rod are constant, while the compliance matrix of the branch's upper rod is variable, which is related to the change of the branch length. Thus, a coefficient λ_i is introduced, then the i-th (i=1,2,3,4) branch's upper rod compliance matrix $\boldsymbol{C}_{is}$ of the mechanism can be written as:

$$\boldsymbol{C}_{is}=\begin{bmatrix} \frac{1}{k_f\lambda_i^3} & 0 & 0 & 0 & \frac{3}{2k_f l_{is}\lambda_i^2} & 0 \\ 0 & \frac{1}{k_f\lambda_i^3} & 0 & -\frac{3}{2k_f l_{is}\lambda_i^2} & 0 & 0 \\ 0 & 0 & \frac{1}{k_a\lambda_i} & 0 & 0 & 0 \\ 0 & -\frac{3}{2k_f l_{is}\lambda_i^2} & 0 & \frac{3}{k_f l_{is}^2\lambda_i} & 0 & 0 \\ \frac{3}{2k_f l_{is}\lambda_i^2} & 0 & 0 & 0 & \frac{3}{k_f l_{1s}^2\lambda_i} & 0 \\ 0 & 0 & 0 & 0 & 0 & \frac{1}{k_t\lambda_i} \end{bmatrix}, \tag{3}$$

where λ_i is the length ratio, $\lambda_i = l_{is}/\ l_{is0}$. And l_{is0} is the upper rod's length of the i-th branch, l_{is} is the initial length of the upper rod in the i-th branch, k_f is the bending stiffness of the upper rod; k_a is the axial stiffness of the upper rod; k_t is the torsional stiffness of the rod.

Taking the 2RPU/UPR PM as an example, the moving platform's linear deformation and torsional deformation under the action of external force will be solved below.

The relationship between the deformation and external force of the i-th branch's end is:

$$\boldsymbol{X}_i = \boldsymbol{C}_i\boldsymbol{F}_i, \tag{4}$$

where, $\boldsymbol{F}_i$ is the applied force at the end of the i-th branch, $\boldsymbol{X}_i$ is the total deformation at the end of the i-th branch, $\boldsymbol{C}_i$ is the whole compliance matrix of the i-th branch.

The relationship between the force $\boldsymbol{F}_{ij}$ applied at the point a_{ij} and the applied force $\boldsymbol{F}_i$ at the point a_i in the i-th branch shown in Figure 3 can be expressed as

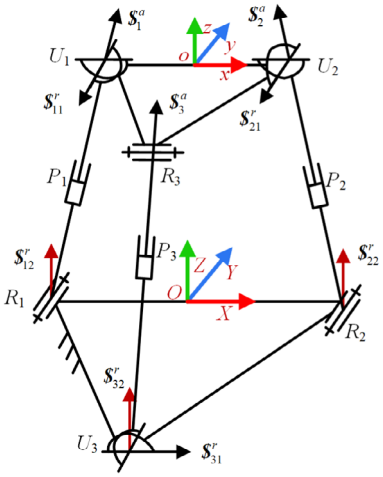

(a) 2RPU/UPR mechanism

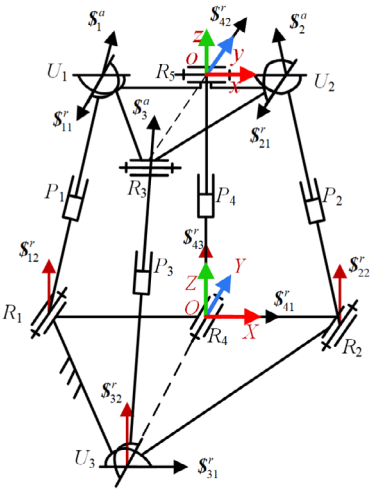

(b) 2RPU/UPR/RPR mechanism

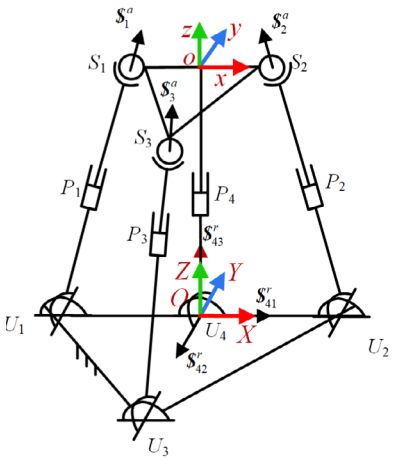

(c) 3UPS/UP mechanism

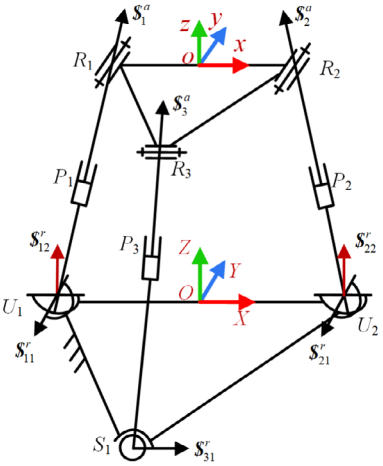

(d) 2UPR/SPR mechanism

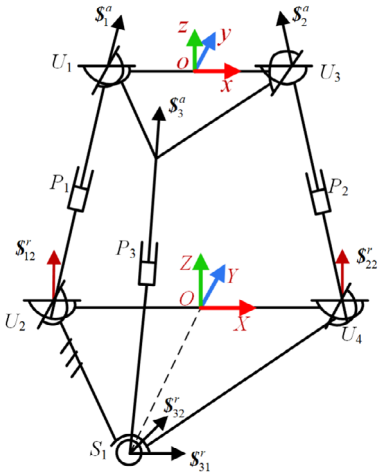

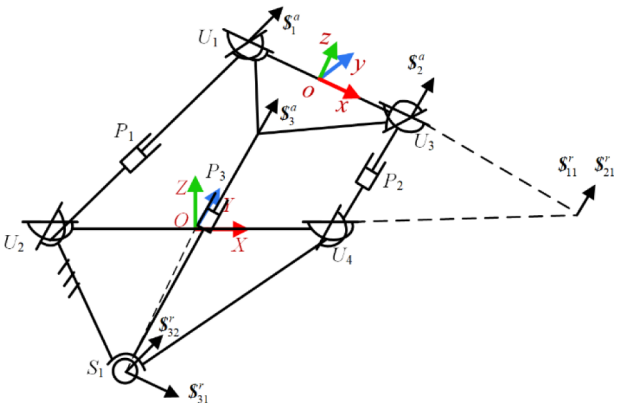

(e) 2UPU/SP mechanism

Figure 2 Schematic configurations of five 2R1T PMs

Table 1 Structure parameters of parallel mechanisms

Parameter	Value
$2a$	0.3 m
$2b$	0.18 m
φ	70°
μ	0.3
h	0.335 m
l_{i1} (i=1,2,3,4)	0.18 m
d_{i1}	0.0155 m
d_{i2}	0.02 m
d_p	0.016 m
l_p	0.02 m

$$\boldsymbol{F}_{ij} = {}^{j}\boldsymbol{J}_i \boldsymbol{F}_i, \tag{5}$$

where ${}^{j}\boldsymbol{J}_i$ is the force transformation matrix between $\boldsymbol{F}_i$ and $\boldsymbol{F}_{ij}$, which can be expressed as

$${}^{j}\boldsymbol{J}_i = \begin{bmatrix} {}^{j}_{i}\boldsymbol{R} & 0 \\ S({}^{j}_{i}\boldsymbol{P}){}^{j}_{i}\boldsymbol{R} & {}^{j}_{i}\boldsymbol{R} \end{bmatrix}, \tag{6}$$

${}^{j}_{i}\boldsymbol{R}$ represents the orientation matrix of the frame a_i-$u_iv_iw_i$ attached at point a_i with respect to frame a_{ij}-$u_{ij}v_{ij}w_{ij}$ attached at point a_{ij}, ${}^{j}_{i}\boldsymbol{P}$ denotes the position vector from point a_{ij} to a_i in the frame a_{ij}-$u_{ij}v_{ij}w_{ij}$, $S({}^{j}_{i}\boldsymbol{P})$ is the anti-symmetric matrix composed of vector ${}^{j}_{i}\boldsymbol{P}$.

The deformation $\boldsymbol{X}_{ij}$ at point a_{ij} can be calculated under the action of force $\boldsymbol{F}_{ij}$ applied at the joint j:

$$\boldsymbol{X}_{ij} = \boldsymbol{C}_{ij}\boldsymbol{F}_{ij}. \tag{7}$$

Substituting Eqs. (5) ~ (7) into Eq. (4), the deformation of the i-th branch's end can be formulated as:

$$\boldsymbol{X}_i = \sum_{j=1}^{3} \boldsymbol{J}_{ij}\boldsymbol{X}_{ij} = \sum_{j=1}^{3} \boldsymbol{J}_{ij}\boldsymbol{C}_{ij}{}^{j}\boldsymbol{J}_i F_i = \sum_{j=1}^{3} {}^{j}\boldsymbol{J}_i^{\mathrm{T}}\boldsymbol{C}_{ij}{}^{j}\boldsymbol{J}_i\boldsymbol{F}_i. \tag{8}$$

Supposed that $\boldsymbol{C}_x$ represents the compliance matrix of branch's lower rod, $\boldsymbol{C}_R$ represents the compliance matrix of R joint, $\boldsymbol{C}_P$ represents the compliance matrix of prismatic joint. Based on Eq. (8), the deformation at the end of the $\mathrm{R_1P_1U_1}$ branch can be calculated as

$$\begin{cases} \boldsymbol{X}_1 = \left({}^{1}\boldsymbol{J}_1^{\mathrm{T}}\boldsymbol{C}_{11}{}^{1}\boldsymbol{J}_1 + {}^{2}\boldsymbol{J}_1^{\mathrm{T}}\boldsymbol{C}_{12}{}^{2}\boldsymbol{J}_1 + {}^{3}\boldsymbol{J}_1^{\mathrm{T}}\boldsymbol{C}_{13}{}^{3}\boldsymbol{J}_1\right)\boldsymbol{F}_1, \\ \boldsymbol{C}_{11} = \boldsymbol{J}_x\boldsymbol{C}_R\boldsymbol{J}_x^{\mathrm{T}} + \boldsymbol{J}_y\boldsymbol{C}_R\boldsymbol{J}_y^{\mathrm{T}} + \boldsymbol{C}_x, \\ \boldsymbol{C}_{12} = \boldsymbol{C}_P + \boldsymbol{C}_{1s}, \\ \boldsymbol{C}_{13} = \boldsymbol{J}_x\boldsymbol{C}_R\boldsymbol{J}_x^{\mathrm{T}}, \end{cases} \tag{9}$$

where $\boldsymbol{J}_x = \begin{bmatrix} \boldsymbol{R}(x,\pi/2) & \\ & \boldsymbol{R}(x,\pi/2) \end{bmatrix}$, $\boldsymbol{J}_y = \begin{bmatrix} \boldsymbol{R}(y,\pi/2) & \\ & \boldsymbol{R}(y,\pi/2) \end{bmatrix}$, ${}^{2}\boldsymbol{J}_1 = \begin{bmatrix} {}^{2}_{1}\boldsymbol{R} & 0 \\ S({}^{2}_{1}\boldsymbol{P}){}^{2}_{1}\boldsymbol{R} & {}^{2}_{1}\boldsymbol{R} \end{bmatrix}$, ${}^{3}\boldsymbol{J}_1 = \begin{bmatrix} {}^{3}_{1}R & 0 \\ S({}^{3}_{1}P){}^{3}_{1}R & {}^{3}_{1}R \end{bmatrix}$.

Then the deformation of the branch's end along the direction of the constraint force can be expressed as:

$$\boldsymbol{X}_f^1 = \boldsymbol{G}_f^{1\mathrm{T}}\left(\boldsymbol{J}_{11}\boldsymbol{C}_{11}{}^{1}\boldsymbol{J}_1 + \boldsymbol{J}_{12}\boldsymbol{C}_{12}{}^{1}\boldsymbol{J}_2 + \boldsymbol{J}_{13}\boldsymbol{C}_{13}{}^{1}\boldsymbol{J}_3\right)\boldsymbol{F}_1, \tag{10}$$

where $\boldsymbol{G}_f^1$ is the unit screw system expressed in the frame a_1-$u_1v_1w_1$, $\boldsymbol{G}_f^1 = \left[\ \$_{11}^{r}\ \ \$_{12}^{r}\ \ \$_{1}^{a}\ \right]$.

At the same time, the force $\boldsymbol{F}_1$ can be expressed as:

$$\boldsymbol{F}_1 = \boldsymbol{G}_f^1\boldsymbol{f}_1. \tag{11}$$

Substituting Eq. (11) into Eq. (10), $\boldsymbol{X}_f^1$ can be expressed as:

$$\boldsymbol{X}_f^1 = \boldsymbol{G}_f^{1\mathrm{T}}\left(\boldsymbol{J}_{11}\boldsymbol{C}_{11}{}^{1}\boldsymbol{J}_1 + \boldsymbol{J}_{12}\boldsymbol{C}_{12}{}^{1}\boldsymbol{J}_2 + \boldsymbol{J}_{13}\boldsymbol{C}_{13}{}^{1}\boldsymbol{J}_3\right)\boldsymbol{G}_f^1\boldsymbol{f}_1. \tag{12}$$

Then the stiffness of the $\mathrm{R_1P_1U_1}$ branch can be obtained:

$$\boldsymbol{K}_1 = \left(\boldsymbol{G}_f^{1\mathrm{T}}\left(\boldsymbol{J}_{11}\boldsymbol{C}_{11}{}^{1}\boldsymbol{J}_1 + \boldsymbol{J}_{12}\boldsymbol{C}_{12}{}^{1}\boldsymbol{J}_2 + \boldsymbol{J}_{13}\boldsymbol{C}_{13}{}^{1}\boldsymbol{J}_3\right)\boldsymbol{G}_f^1\right)^{-1}. \tag{13}$$

In Refs. [71, 72], the over-constraint wrench system and the spatial composite elastic deformation of the branch members of the parallel mechanism were considered, the whole stiffness matrix of the PMs was

Table 2 Definition of four types of branch stiffness

Influencing factors		Defining values of stiffness	Influencing factors		Defining values of stiffness
Structure stiffness of rod	Axial stiffness	2.8 KN/mm	Structural stiffness of P joint	Flexural stiffness	2.6 KN/mm
	Flexural stiffness	0.65 KN/mm		Torsional stiffness	8 KN · mm/rad
	Torsional stiffness	4.4 KN · mm/rad	Drive structure stiffness	Axial stiffness	3 KN/mm
Structural stiffness of R joint	Tension and compression stiffness	4 KN/mm		Flexural stiffness	0.2 KN/mm
	Torsional stiffness	3.5 KN·mm/rad		Torsional stiffness	7.5 KN·mm/rad

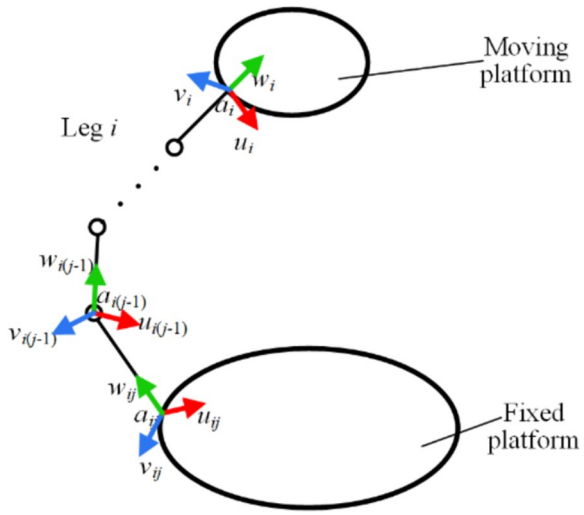

Figure 3 The coordinates in the *i*-th branch

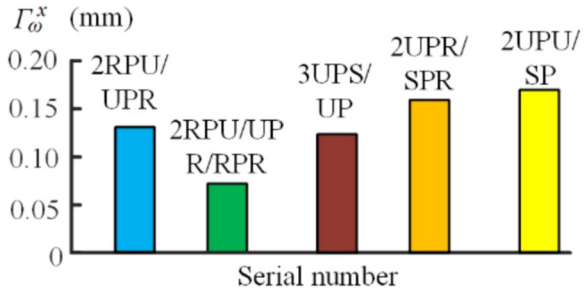

Figure 4 The linear deformation of each mechanism in the *x*-direction

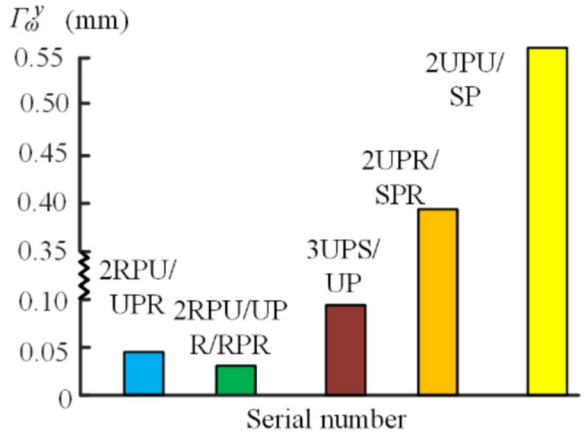

Figure 5 The linear deformation of each mechanism in the *y*-direction

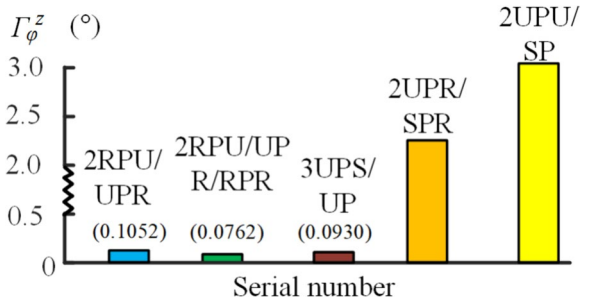

Figure 6 The torsional deformation of each mechanism around the *z*-direction

established, and the general analytical expression of this type of mechanism was obtained:

$$\boldsymbol{K} = \boldsymbol{G}_f^F \boldsymbol{K}_i (\boldsymbol{G}_f^F)^{\mathrm{T}}, \tag{14}$$

where $\boldsymbol{G}_f^F$ is the mapping matrix of the helical magnitude $\boldsymbol{f}$ of each constraint force of the parallel mechanism and the external force $\boldsymbol{F}$ of the parallel mechanism; $\boldsymbol{K}_i$ is the stiffness matrix of the *i*-th branch of the parallel mechanism.

Under the action of external force $\boldsymbol{F}$, the deformation $\boldsymbol{D}$ of the moving platform and the external force $\boldsymbol{F}$ have the following relationship:

$$\boldsymbol{F} = \boldsymbol{K}\boldsymbol{D}. \tag{15}$$

For five different mechanisms, variation range of the angles α and β are confined to $[-\pi/6 \sim \pi/6]$ and $[-\pi/9 \sim \pi/9]$, respectively, which can be obtained based on the workspace of the PMs. At the same time, the parameter h of the parallel mechanism is set to be 0.335 m. Using the principle of the "layered slice", the linear deformation distribution of the moving platform of the mechanism can be obtained combined with the inverse position solution.

Under the action of an external load with 10 N exerted on the origin of the moving coordinate system along the *x*-direction, each PM's linear deformation in the *x*-direction is calculated based on Eq. (1), as shown in Figure 4.

Similarly, under the action of an external load with 10 N exerted on the origin of the moving coordinate system along the *y*-direction, each PM's linear deformation in the *y*-direction is calculated based on Eq. (1), as shown in Figure 5.

Under the action of an external load with 10 N·m exerted on the origin of the moving coordinate system around the *z*-direction, each mechanism's angular deformation in the *z*-direction is calculated based on Eq. (2), as shown in Figure 6.

4.2 Comparative Analysis of Stiffness and Selection of the Optimal Mechanism

(1) *Comparative analysis of bending stiffness along the x-direction:* By observing the average linear deformation of the five parallel mechanisms in the x-direction, 2RPU/UPR/RPR PM has the smallest average deformation in the x-direction, followed by 2RPU/UPR PM, 3UPS/UP PM, 2UPR/SPR PM, and 2UPU/SP PM has the largest linear deformation.

(2) *Comparative analysis of the bending stiffness along the y-direction:* By observing the average linear deformation of the five parallel mechanisms in the y-direction, 2RPU/UPR/RPR PM has the smallest average deformation in the x-direction, followed by 2RPU/UPR PM, 3UPS/UP PM, 2UPR/SPR PM, and 2UPU/SP PM has the largest linear deformation.

(3) *Comparative analysis of torsional stiffness in z-direction:* By observing the average angular deformation of the five parallel mechanisms in the z-direction, 2RPU/UPR/RPR PM has the smallest average deformation in the z-direction, followed by 3UPS/UP PM, 2RPU/UPR PM, 2UPR/SPR PM, and 2UPU/SP PM has the largest linear deformation.

By comparing the data in Figures 4, 5, 6, the 2RPR/UPR/RPR mechanism obtains better bending stiffness in the x and y-directions and torsional stiffness in the z-direction than the other four PMs. Therefore, the mechanism can preferably be used as the PM part of the five-DOF hybrid machining robot.

In what follows, the influence factors of the configuration stiffness will be analysed from the point of constraint forces and deformations of the branches, thus the correctness of the above conclusions can be verified.

5 Force and Deformation Analysis of the Branches

5.1 Force Analysis of the Branches

Considering redundant and typical constraints, the force analysis of the over-constrained PMs is a statically indeterminate problem with complicated calculations. Accordingly, an analysis method based on ADAMS simulation software is applied in the present study. In this regard, a method [47] has been proposed to establish the rigid-flexible coupling simulation model of over-constrained PMs. However, the simulation model can only stay in a single configuration when PMs contain translational joints. In other words, this method cannot realize the force simulation in the whole workspace. In order to resolve this shortcoming, an improved method is proposed to establish the rigid-flexible simulation model of over-constrained PMs and realize the continuous force simulation analysis of the PMs in the whole workspace based on the method proposed in Ref. [47].

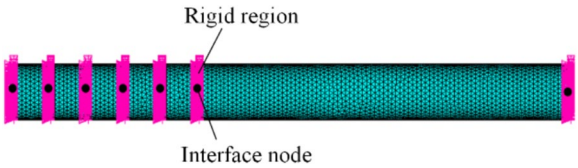

Figure 7 Flexible model of the slider containing multiple interface nodes

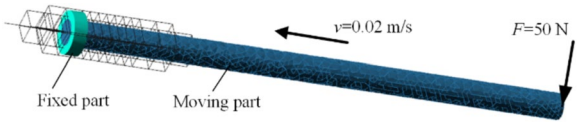

Figure 8 Established model in the Adams environment for the prismatic joint

Accordingly, the rigid-flexible coupling model of the over-constrained mechanism has been established in ADAMS software. It is assumed that the moving platform and the fixed platform are rigid bodies, while the connecting links are flexible bodies. For the revolute joints, including the universal joints and the spherical joints, since the position of the rotating axis does not change relative to the rotating links, the position of the interface node within the modal center file relative to the link is fixed. Consequently, only one interface node should be set to connect the position of each revolute joint and simulate the revolute contact. However, for prismatic joints such as the guide rail and the slider, when the slider translates relative to the guide rail, the contact position between the guide rail and the slider constantly changes during the movement. In ADAMS software, since only a single position can be chosen when establishing the kinematic joints in the flexible body, only the force performance of prismatic joints in the current state can be simulated, and the entire sliding process cannot be simulated. If multiple interface nodes are set up for the prismatic joints in the modal neutral file, P joints can be established for the slider and the guide rail at each node position. In the simulation process, when the slider moves to a specific position relative to the guide rail, the prismatic joints at the corresponding node position are set to be activated, and the other joints are deactivated. Similarly, when the slider moves to the next position, the prismatic joints in the previous position become invalid, while the prismatic joints in the current position become effective. The whole process can be considered the discretized contact position of the flexible body into multiple

Table 3 Settings of parameters of the flexible model of the P joint

Parameter	Value
D	0.015 m
L	0.3 m
E	2.1×10^5 MPa
v	0.02 m/s
t	5 s
F	50 N

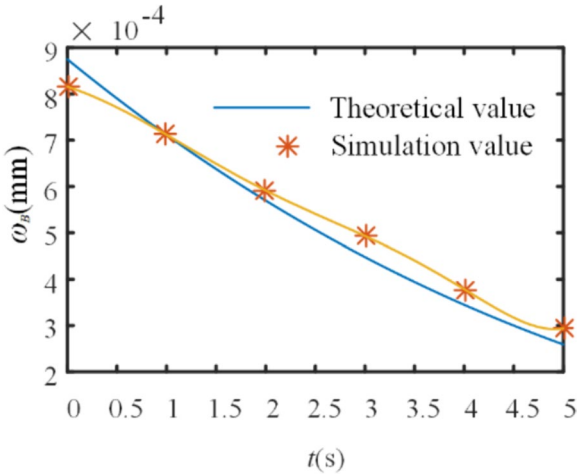

Figure 9 Distributions of the cantilever deformation

interface nodes. The greater the discretization degree, the more accurate the simulation results, but the greater the corresponding computational costs. Multiple interface nodes the discretization degree.

Figure 7 illustrates the established flexible model of the slider containing multiple interface nodes. The calculation process is as follows.

At the first step, the multiple interface nodes were introduced to ADAMS software, and then the joints, driver, and external force were applied to the interface nodes of the slider. Meanwhile, the prismatic joints and drivers were exerted to middle multiple interface nodes, which show in Figure 8.

The calculations assume that the slider is a cylindrical rod with a diameter D and length L. Moreover, the translational speed, motion time, and the applied force to the end of the slider are v, t, and F, respectively. The slider can be simplified to a cantilever beam, and the end deformation along the force axis F can be calculated. When the slider moves to the left, the end deformation gradually decreases because the cantilever's length gradually decreases during the movement.

Deformation of the cantilever end can be calculated through the following Eq. (16):

$$w_B = (FL^3)/(3EI), \tag{16}$$

where $I=\pi D^4/64$ and E are the moment of inertia of the slider and modulus of elasticity, respectively. Table 3 is the flexible model of the P joint's settings of parameters.

Deformation of the cantilever end can then be obtained either from simulations or Eq. (16). Figure 9 presents the obtained results accordingly.

Figure 9 reveals that the theoretical and simulation values are consistent, the maximum error between them is less than 6%, resulting from the discretization degree of interface nodes and finite element size, verifying the accuracy of the established model for the prismatic joint in ADAMS software.

Based on the modeling mentioned above method, the rigid-flexible coupling model of the five PMs is established. Figure 10(a)–(e) shows the established models for five types of 2R1T PMs, which can realize the force simulation analysis in the continuous motion process.

In the moving coordinate system o-xyz, the load $\$_F$= (10 N 10 N 10 N; 10 N · m 10 N · m 10 N · m) is applied on the origin of the moving platform for the 2RPU/UPR mechanism. The following motion trajectory is considered in the simulations for the moving platform:

$$\begin{cases} P(x) = 0, \\ P(y) = 0, \\ P(z) = 0.335 + 0.005t, \end{cases} \tag{17}$$

where t=0~1 s is the motion time.

Figure 11(a)–(c) shows variations of the magnitude of driving and constraint force/couple obtained from the rigid-flexible coupling simulations.

In Fig. 11, $f_{a,i}$ represents the magnitude of the driving force of the i-th branch, $f_{r,i}$ the magnitude of the constraint force of the i-th branch, $m_{r,i}$ the magnitudes of the constraint couple of the i-th branch for the 2RPU/UPR mechanism.

In order to verify the analysis accuracy, the weighted generalized inverse method [71, 72] is used to analyse the theoretical force of the typical over-constrained PMs. Equation (18) can be expressed as follows.

$$\boldsymbol{f} = \boldsymbol{W}^{-1}(\boldsymbol{G}_f^F)^{\mathrm{T}}(\boldsymbol{G}_f^F\boldsymbol{W}^{-1}(\boldsymbol{G}_f^F)^{\mathrm{T}})^{\mathrm{T}}\$_F, \tag{18}$$

where $\boldsymbol{G}_f^F$ is the mapping matrix from $\boldsymbol{f}$ to $\$_F$, $\$_F$ is the external force/torque applied on the moving platform, $\boldsymbol{f}$ is the column vector composed of the magnitudes of the driving and constraint force/couple, and $\boldsymbol{W}$ is the weighting matrix determined by the structural stiffness of each branch.

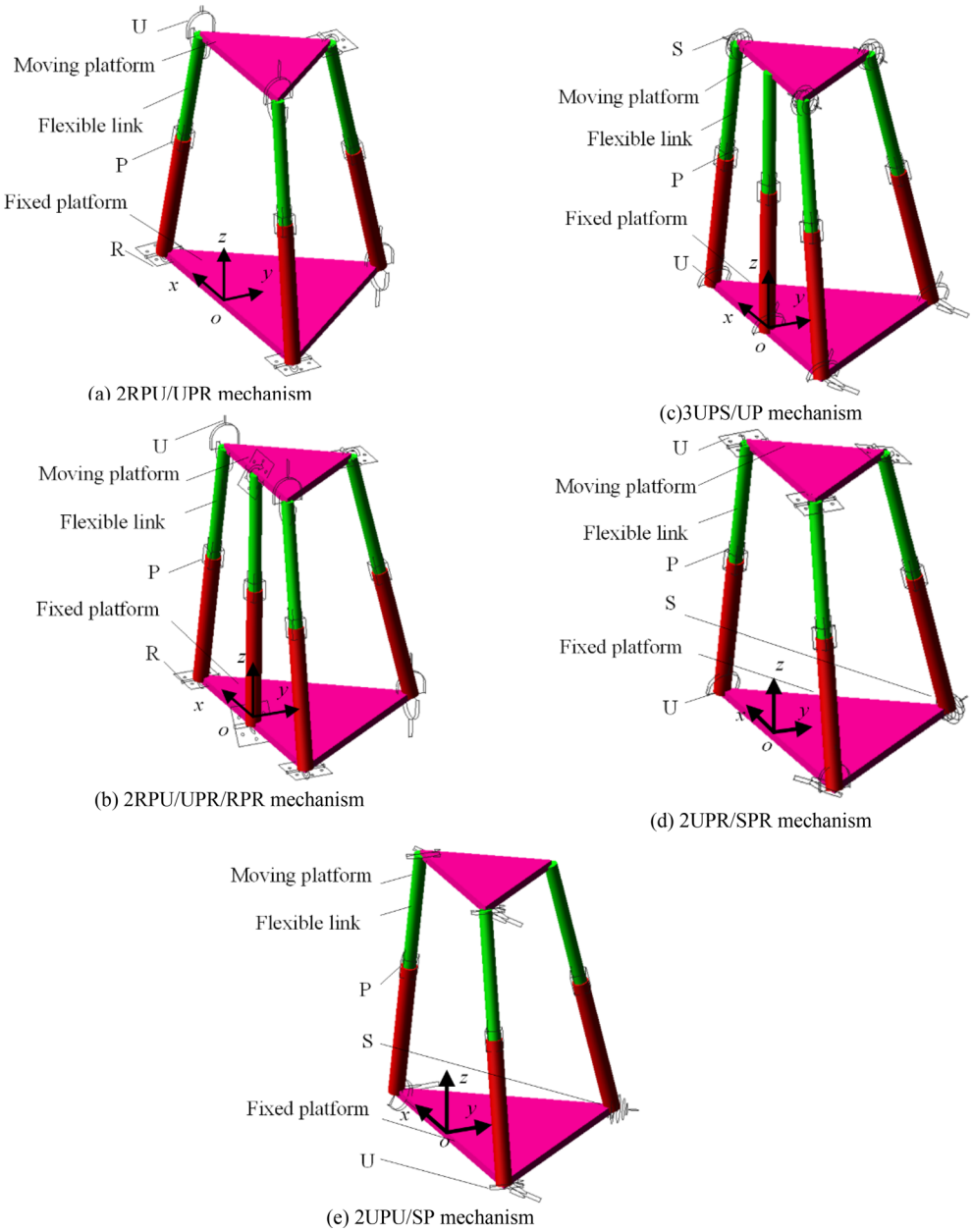

Figure 10 Rigid-flexible coupling models of five types of 2R1T PMs

When the mechanism is in the initial state (i.e., t= 0 s and α=β=0°), magnitudes of the driving force and constraint force/a couple of each branch obtained from simulations and theoretical calculations are listed in Table 4.

It is observed that the error between the theoretical and simulation value is tiny, demonstrating the accuracy of the theoretical and simulation analysis.

Similarly, the accuracy of the other four mechanisms can be verified.

5.2 Comparison of the Branch's Constraint Force/Couple

Using the principle of the "layered slice", the average amplitude of each branch's driving and constraint force/couple of the parallel mechanism at a certain height is obtained combined with the inverse position solution based on the abovementioned method.

Table 5 gives the average magnitude of each branch's the driving and constraint forces/couples of each parallel mechanism in the entire workspace when h=0.335 m,

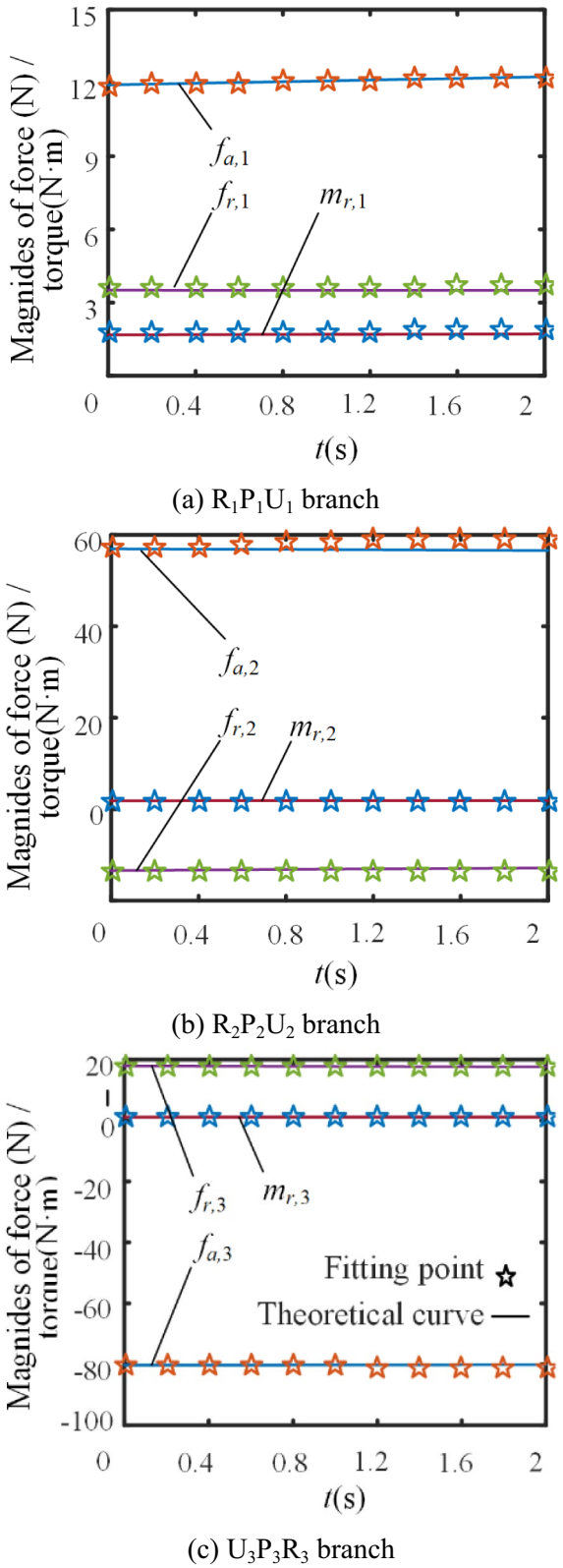

Figure 11 Variations of the magnitudes of the driving and constraint forces/couples

under the action of a lateral force $\$_{Fx}$= (10 N 0 0; 0 0 0) exerted on the moving platform's origin.

In Table 6, 2UPU/SP (2) means that the mechanism is at the position where the x and X-axis intersect, $\$^r_{12}$ and $\$^r_{22}$ are **0**; 2UPU/SP (1) means that the mechanism is at the position where the x and X-axis are parallel, $\$^r_{11}$ and $\$^r_{21}$ are **0**. The position of the 2UPU/SP (1) occupies a small part of the workspace under the designation, so the PM's branch deformation is mainly determined by the deformation at the 2UPU/SP (2) position.

Table 6 gives the average magnitude of each branch's the driving and constraint forces/couples of each parallel mechanism in the entire workspace when h=0.335 m under the action of a lateral force $\$_{Fy}$= (0 10 N 0; 0 0 0) exerted on the moving platform's origin.

Table 7 gives the average magnitude of each branch's the driving and constraint forces/couples of each parallel mechanism in the entire workspace when h=0.335 m under the action of a lateral force $\$_{Fz}$= (0 0 0; 0 0 10 N·mm) exerted on the moving platform's origin.

In the first column of Tables 5, 6 and 7, the branches 1, 2, and 3 in the horizontal axis for the 2RPU/UPR mechanism represent $R_1P_1U_1$, $R_2P_2U_2$, and $U_3P_3R_3$ branches, respectively. Moreover, for the 2RPU/UPR/RPR mechanism, the branches 1, 2, 3, and 4 represent $R_1P_1U_1$, $R_2P_2U_2$, $U_3P_3R_3$, and $R_4P_4R_4$ branches, respectively. For the 3UPS/UP mechanism, the branches 1, 2, 3, and 4 represent $U_1P_1S_1$, $U_2P_2S_2$, $U_3P_3S_3$, and U_4P_4 branches, respectively. For the 2UPR/SPR mechanism, the branches 1, 2, and 3 represent $U_1P_1R_1$, $U_2P_2R_2$, and $S_3P_3R_3$ branches, respectively. For the 2UPU/SP mechanism, the branches 1, 2, and 3 represent $U_{11}P_1U_{12}$, $U_{21}P_2U_{22}$, and S_3P_3 branches, respectively.

By observing Tables 5, 6, 7, we can get the magnitudes of the driving and constraint forces/couples on the branches of the five PMs under the action of same external force. By comparing the magnitudes of the driving and constraint forces/couples on the same branch, the main factors affecting the deformation of the branch can be obtained.

1. Comparative analysis of the driving and constraint forces/couples of branches under the action of external force $\$_{Fx}$.

The reason of this result would be analyzed from the point of constraint force/couple supplied by the branches, since the axial stiffness of the limb is relatively large.

It can be seen from Table 5 that when the same external force $\$_{Fx}$ is applied on the moving platform origin, the

Table 4 Obtained results for each branch of the 2RPU/UPR mechanism

Branch	Driving and constraint force/torque	Theoretical value	Simulation value	Absolute error	Relative error
$R_1P_1U_1$	$f_{a,1}$	11.9204 N	11.89 N	0.0304	0.26%
	$f_{r,1}$	3.5066 N	3.648 N	− 0.1414	− 3.88%
	$m_{r,1}$	1.6756 N · m	1.748 N · m	− 0.0724	− 4.14%
$R_2P_2U_2$	$f_{a,2}$	56.9591 N	57 N	− 0.0409	− 0.07%
	$f_{r,2}$	− 13.4071 N	− 13.57 N	0.1629	− 1.20%
	$m_{r,2}$	1.8637 N · m	1.942 N · m	− 0.0783	− 4.03%
$U_3P_3R_3$	$f_{a,3}$	− 80.3067 N	− 80.34 N	0.0324	− 0.04%
	$f_{r,3}$	17.9403 N	17.88 N	0.0603	0.34%
	$m_{r,3}$	1.0953 N · m	1.039 N · m	0.0563	5.42%

Table 5 The magnitude of the driving and constraint wrenches under the action of force $\$_{Fx}$

Branch		2RPU/UPR	2RPU/UPR/RPR	3UPS/UP	2UPR/SPR	2UPU/SP (2)	2UPU/SP(1)
1	$\$_1^a$	12.4316 N	12.4316 N	12.7133 N	12.6695 N	12.9594 N	10.0860 N
	$\$_{11}^r$	0.0059 N	0.0027 N	/	1.2362 N	1.08315 N	/
	$\$_{12}^r$	1.1125 N·mm	0.4437 N·mm	/	1.4794 N·mm	/	1.5453 N·mm
2	$\$_2^a$	12.4316 N	12.4316 N	12.7133 N	12.6695 N	12.9594 N	10.0860 N
	$\$_{21}^r$	0.0059 N	0.0027 N	/	1.2362 N	1.08315 N	/
	$\$_{22}^r$	1.1125 N·mm	0.4437 N·mm	/	1.4794 N·mm	/	1.5453 N·mm
3	$\$_3^a$	0.0000 N	0.0000 N	0.9206 N	4.5485 N	3.9246 N	3.0666 N
	$\$_{31}^r$	13.7295 N	6.8125 N	/	13.6268 N	13.6978 N	14.0000 N
	$\$_{32}^r$	0.7151 N·mm	0.1414 N·mm	/	/	1.318 N	0.6706 N
4	$\$_{41}^r$	/	6.9169 N	13.7286 N	/	/	/
	$\$_{42}^r$	/	0.0008 N	0.8313 N	/	/	/
	$\$_{43}^r$	/	0.4301 N·mm	0.0064 N·mm	/	/	/

Table 6 The magnitude of the driving and constraint wrenches under the action of force $\$_{Fy}$

Branch		2RPU/UPR	2RPU/UPR/RPR	3UPS/UP	2UPR/SPR	2UPU/SP (2)	2UPU/SP (1)
1	$\$_1^a$	0.8951 N	0.8951 N	8.7044 N	8.6215 N	8.7827 N	8.4171 N
	$\$_{11}^r$	4.8941 N	3.5123 N	/	6.9852 N	0.0575 N	/
	$\$_{12}^r$	0.1511 N·mm	0.0960 N·mm	/	0.4961	/	0
2	$\$_2^a$	0.8951 N	0.8951 N	8.7044 N	8.6215 N	8.7827 N	8.4171 N
	$\$_{21}^r$	4.8941 N	3.5123 N	/	6.9852 N	0.0575 N	/
	$\$_{22}^r$	0.1511 N·mm	0.0960 N·mm	/	0.4961 N·mm	/	0
3	$\$_3^a$	0.0000 N	0.0000 N	17.6524 N	17.1598 N	19.5235 N	13.6461 N
	$\$_{31}^r$	0.0173 N	0.0092 N	/	0.2389 N	0.2484 N	0.0000 N
	$\$_{32}^r$	0.0954 N·mm	0.0529 N·mm	/	/	13.5323 N	13.5233 N
4	$\$_{41}^r$	/	0.0082 N	0.1699 N	/	/	/
	$\$_{42}^r$	/	2.7635 N	16.9696 N	/	/	/
	$\$_{43}^r$	/	0.0489 N·mm	0.0330 N·mm	/	/	/

constraint force mainly resisting the external force for the 2RPU/UPR PM is $\$_{31}^r$, the constraint forces mainly resisting the external force for the 2RPU/UPR/RPR PM are $\$_{31}^r$ and $\$_{41}^r$, the constraint force mainly resisting the external force for the 3UPS/UP PM is $\$_{41}^r$, the constraint forces mainly resisting the external force for the 2UPR/SPR PM

Table 7 The magnitude of the driving and constraint wrenches under the action of force $\$_{Fz}$

Branch		2RPU/UPR	2RPU/UPR/RPR	3UPS/UP	2UPR/SPR	2UPU/SP (2)	2UPU/SP (1)
1	$\$_1^a$	6.2362 N	6.2362 N	6.4476 N	7.1979 N	6.88635 N	6.4895 N
	$\$_{11}^r$	0.0171 N	0.0150 N	/	1.9936 N	3.7998 N	/
	$\$_{12}^r$	3.2295 N·mm	2.4341 N·mm	/	5.2238 N·mm	/	5.3114 N·mm
2	$\$_2^a$	6.2362 N	6.2362 N	6.4476 N	11.9263 N	6.88635 N	6.4895 N
	$\$_{21}^r$	0.0171 N	0.0150 N	/	1.9505 N	3.7998 N	/
	$\$_{22}^r$	3.2295 N·mm	2.4341 N·mm	/	5.2258 N·mm	/	5.3114 N·mm
3	$\$_3^a$	0.0000 N	0.0000 N	0.6053 N	15.9690 N	15.2188 N	10.7946 N
	$\$_{31}^r$	1.8832 N	0.9344 N	/	2.1808 N	0.546 N	2.1121 N
	$\$_{32}^r$	3.3261 N·mm	2.5207 N·mm	/	/	4.5226 N	2.3210 N
4	$\$_{41}^r$	/	0.9496 N	1.8826 N	/	/	/
	$\$_{42}^r$	/	0.0041 N	0.5421 N	/	/	/
	$\$_{43}^r$	/	2.3592 N·mm	10.2245 N·mm	/	/	/

are $\$_{11}^r$, $\$_{21}^r$ and $\$_{31}^r$, the constraint forces mainly resisting the external force for the 2UPU/SP PM are $\$_{11}^r$, $\$_{21}^r$, $\$_{31}^r$ and $\$_{32}^r$. Among them, the constraint forces against this external force for the 2RPU/UPR/RPR PM are obviously smaller than that of other parallel mechanisms. Therefore, among the five parallel mechanisms, 2RPU/UPR/RPR has the smallest deformation and the largest stiffness in the *X*-direction.

2. Comparative analysis of the driving and constraint forces/couples of branches under the action of external force $\$_{Fy}$.

It can be seen from Table 6 that when the same external force $\$_{Fy}$ is applied, the constraint forces that mainly resist this external force for the 2RPU/UPR PM are $\$_{11}^r$ and $\$_{21}^r$, the constraint forces that mainly resist this external force for the 2RPU/UPR/RPR PM are $\$_{11}^r$,$\$_{21}^r$ and $\$_{42}^r$, and the constraint force that mainly resist this external force for the 3UPS/UP PM is $\$_{42}^r$, the constraint forces that mainly resist this external force for the 2UPR/SPR PM are $\$_{11}^r$ and $\$_{21}^r$, and the constraint forces that mainly resist this external force for the 2UPU/SP PM are $\$_{11}^r$, $\$_{21}^r$ and $\$_{31}^r$. Among them, the constraint forces against this external force for the 2RPU/UPR/RPR PM are obviously smaller than that of other parallel mechanisms. Therefore, among the five parallel mechanisms, 2RPU/UPR/RPR has the smallest deformation and the largest stiffness in the *Y*-direction.

3. Comparative analysis of the driving and constraint forces/couples of branches under the action of external force $\$_{Fz}$.

It can be seen from Table 7 that when the same external force $\$_{Fz}$ is applied, the constraint forces that mainly resist this external force for the 2RPU/UPR PM are $\$_{12}^r$, $\$_{22}^r$, $\$_{31}^r$ and $\$_{32}^r$, the constraint forces that mainly resist this external force for the 2RPU/UPR/RPR PM are $\$_{12}^r$, $\$_{22}^r$, $\$_{31}^r$, $\$_{32}^r$ and $\$_{43}^r$, and the constraint force that mainly resist this external force for the 3UPS/UP PM is $\$_{43}^r$, the constraint forces that mainly resist this external force for the 2UPR/SPR PM are $\$_{11}^r$, $\$_{12}^r$, $\$_{12}^r$, $\$_{22}^r$ and $\$_{31}^r$, and the constraint forces that mainly resist this external force for the 2UPU/SP PM are $\$_{11}^r$, $\$_{12}^r$, $\$_{21}^r$, $\$_{22}^r$, $\$_{31}^r$ and $\$_{32}^r$.When an external couple is applied to parallel mechanisms, its deformation is complicated, which is the result of the joint action of constraint forces and couples. Therefore, although the constraint couples of 2UPU/SP PM are small, its constraint forces cause large torsional deformation, so its overall deformation is large. For the 3UPS/UP

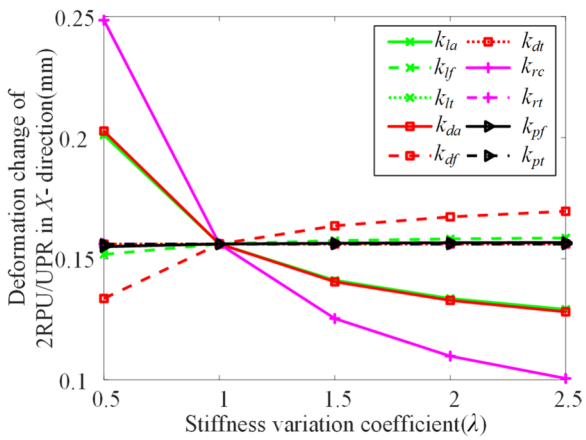

Figure 12 The deformation changes in *X*-direction of 2RPU/UPR PM when the stiffness value changes

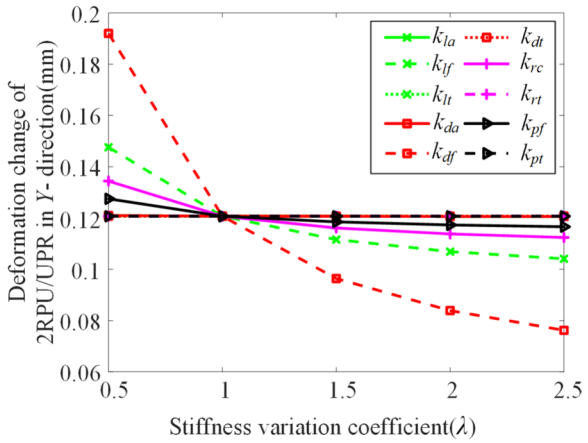

Figure 13 The deformation changes in *Y*-direction of 2RPU/UPR PM when the stiffness value changes

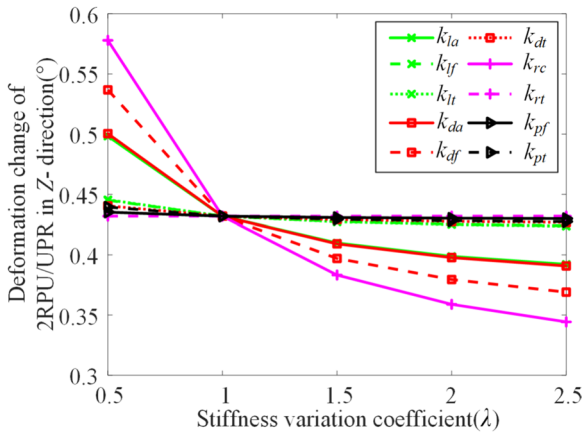

Figure 14 The deformation changes in *Z*-direction of 2RPU/UPR PM when the stiffness value changes

PM, though the value of constraint couple is the largest, there are fewer passive joints within the UP limb, so the torsional deformation caused by the constraint couple is not the largest.

For the 2RPU/UPR, 2RPU/UPR/RPR and 2UPR/SPR PMs, the constraint forces of 2RPU/UPR/RPR PM against this external force are obviously less than that of the other two parallel mechanisms. Therefore, among the five parallel mechanisms, 2RPU/UPR/RPR has the smallest deformation and the largest stiffness in the *Z*-direction.

Therefore, the mechanism 2RPU/UPR/RPR can preferably be used as the PM part of the five-DOF hybrid machining robot, which is consistent with the analysis results in Section 4.

5.3 Effect of Component Stiffness on Overall Stiffness

Taking 2RPU/UPR parallel mechanism as an example, using the control variable method, only the stiffness of a certain component is changed, and the deformation changes of the parallel mechanism in the *X*, *Y*, *Z* directions are observed under the action of a same force.

External force $\$_F$= (10 N 10 N 10 N; 10 N ·m 10 N ·m 10N ·m) exerted on the moving platform origin. When h=0.335 m, the average deformation of the parallel mechanism in the *X*-direction in the entire workspace is shown in the following Figure 12.

In Fig. 12, k_{la} stands for axial stiffness of rod, k_{lf} stands for flexural stiffness of rod, k_{lt} stands for torsional stiffness of rod, k_{da} stands for axial stiffness of drive structure, k_{df} stands for flexural stiffness of drive structure, k_{dt} stands for torsional stiffness of drive structure, k_{rc} stands for tension and compression stiffness of R joint, k_{rt} stands for torsional stiffness of R joint, k_{pf} stands for flexural stiffness of P joint, k_{pt} stands for torsional stiffness of P joint. And stiffness variation coefficient denotes each structure stiffness change multiples, which is a dimensionless value.

Under the action of same external force, when h=0.335 m, the average deformation of the parallel mechanism in the *Y*-direction in the whole workspace is shown in Figure 13.

Under the action of same external force, when h=0.335 m, the average deformation of the parallel mechanism in *Z*-direction in the whole workspace is as shown in Figure 14.

It can be seen from the observation that the *X*-direction deformation of the parallel mechanism is more sensitive to the numerical changes of k_{la}, k_{da} and k_{rc}. The larger the values of k_{la}, k_{da} and k_{rc} are, the smaller the *X*-direction deformation of the parallel mechanism is. The *Y*-direction deformation of the parallel mechanism is sensitive to the numerical changes of k_{lf} and k_{df}. The larger the values of k_{lf} and k_{df} are, the smaller the *Y*-direction deformation of the parallel mechanism is. The *Z*-direction deformation of the parallel mechanism is sensitive to the numerical changes of k_{la}, k_{da}, k_{df} and k_{rc}. The larger the values of k_{la}, k_{da}, k_{df}, and k_{rc} are, the smaller the *Z*-direction deformation of the parallel mechanism is. At the same time, it can be seen from observation that not all stiffness values are greater, the overall stiffness of the parallel mechanism is greater.

Based on the existing stiffness, if the stiffness of the parallel mechanism needs to be improved, the values of k_{la}, k_{da}, k_{df}, and k_{rc} should be increased. Therefore, when designing the structure of parallel mechanism, increasing the section size of the branches, the driving structures and the revolute points can be considered, or

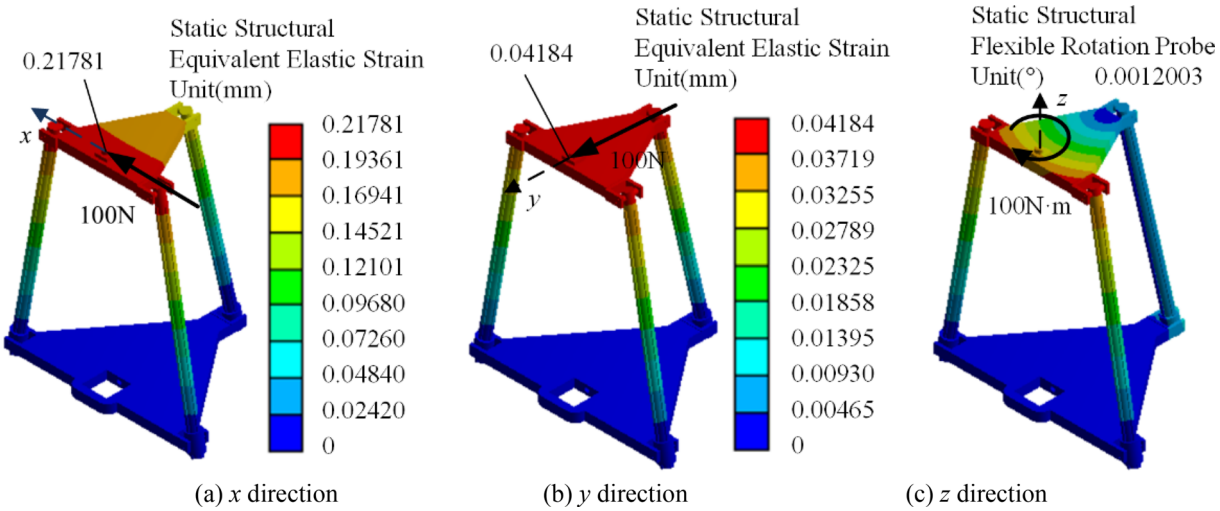

(a) *x* direction (b) *y* direction (c) *z* direction

Figure 15 Deformation of the 2RPU/UPR PM in different directions

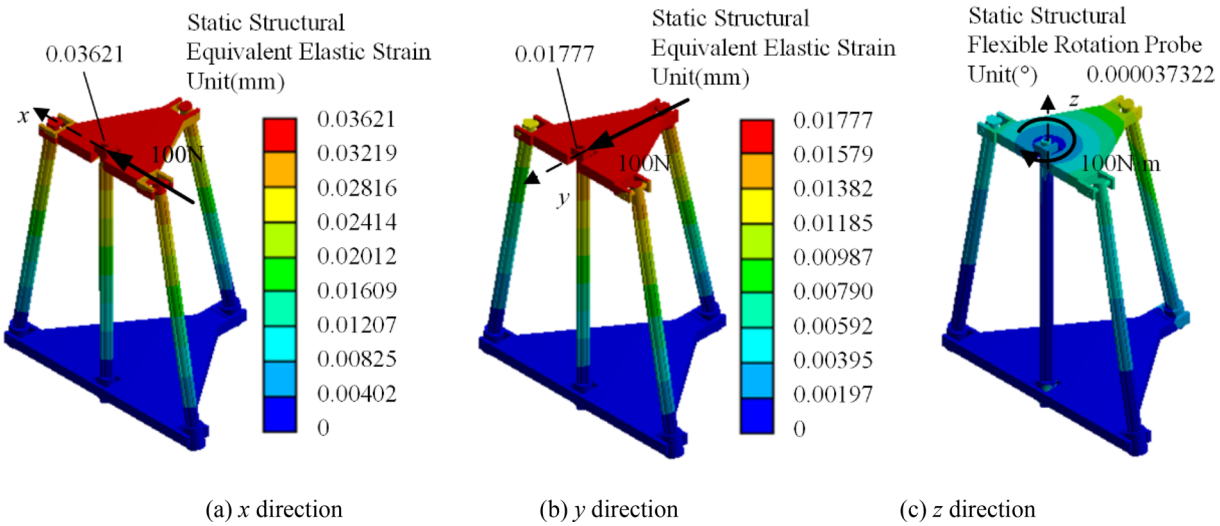

(a) *x* direction (b) *y* direction (c) *z* direction

Figure 16 Deformation of the 2RPU/UPR/RPR PM in different directions

materials with higher strength are used to manufacture these parts.

6 Simulation Verification

In order to verify the correctness and rationality of the proposed stiffness performance indices, considering the five-DOF hybrid processing robot as the application target, simple engineering three-dimensional models of five 2R1T PMs, including 2RPU/UPR, 2RPU/UPR/RPR, 3UPS/SP, 2UPR/SPR, and 2UPU/SP, are established, where the structure of branch screws and screw nuts, branch guide rails and sliding blocks, and revolute joints connecting each branch to the moving and fixed platforms are taken into account. Five simulation calculation models are established by using the Ansys software. It should be indicated that kinematic joints are added, the sliders and the guide rails are locked, and friction is added at each revolute joint. The forces 100 N, 100 N, and a couple of 100 N·m are exerted along the coordinate system's three coordinate axes *x*, *y*, and *z* on the moving platform. The stiffness simulation of the

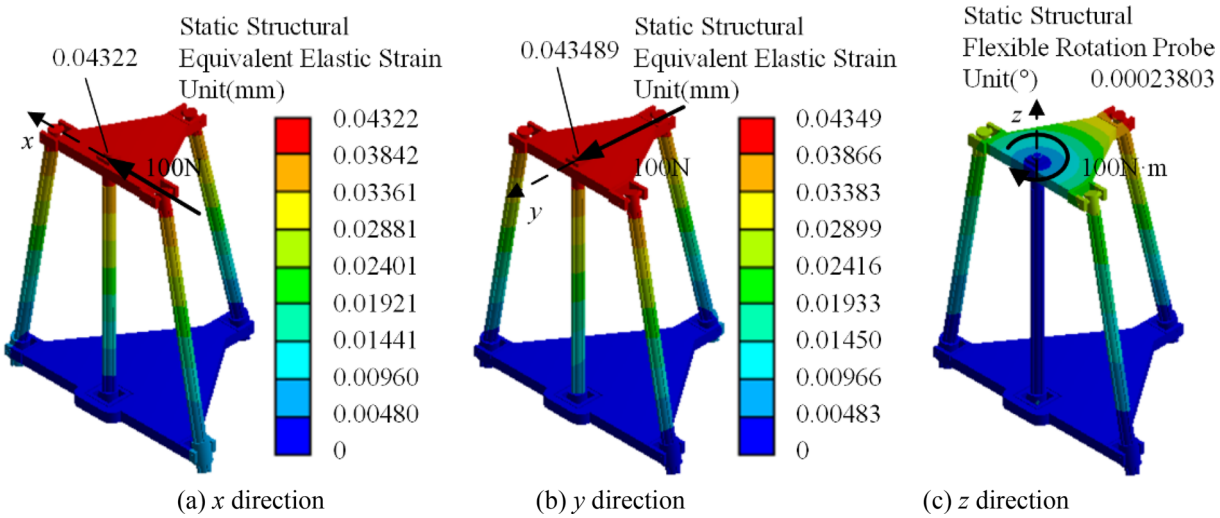

(a) x direction (b) y direction (c) z direction

Figure 17 Deformation of the 3UPS/UP PM in different directions

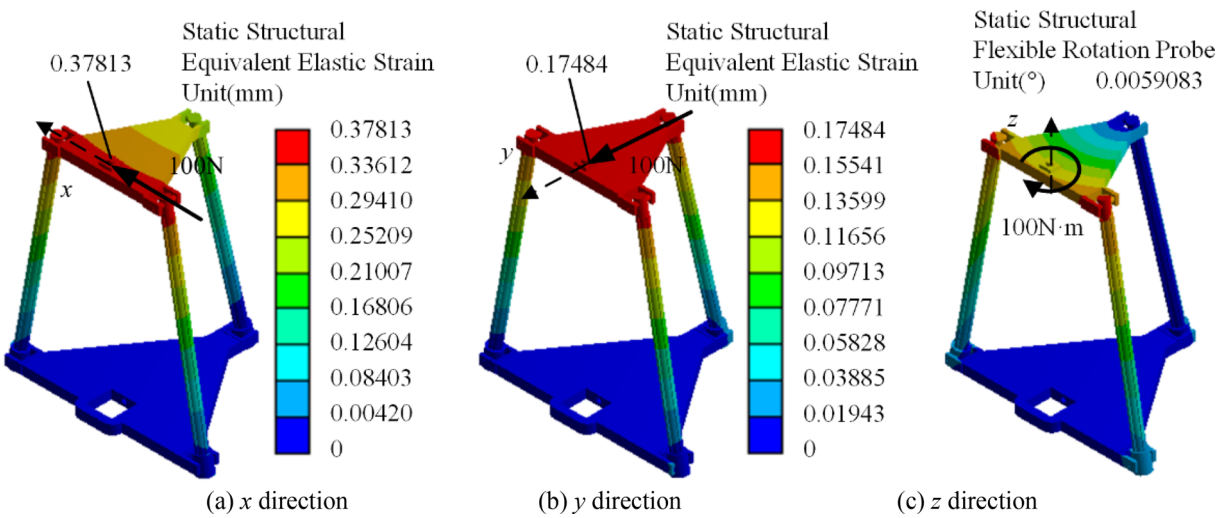

(a) x direction (b) y direction (c) z direction

Figure 18 Deformation of the 2UPR/SPR PM in different directions

PMs of the five hybrid robots is performed. Figures 15, 16, 17, 18, 19 show the obtained results.

To further verify the stiffness analysis results, the stiffness simulation analyses in different configurations are also carried out in the whole workspace. And the maximum deformation in x, y and z-axis, with respect to the variable α, β, and d, are shown in Figures 20, 21, 22, respectively. Where α, β, and d represent rotation angle around the x-axis, rotation angle around the y-axis, and distance from point o to O, respectively. In Figure 20, d and β are kept at a constant, that is, d=290 mm and β=0. In Figure 21, d and α are kept at a constant, that is, d=290 mm and α=0. In Figure 22, α and β are kept at a constant, that is, α=0 and β=0.

It can be seen from Figures 20, 21, 22 that the 2RPR/UPR/RPR mechanism has better bending stiffness in the x and y-directions and torsional stiffness in the z-direction than the other four PMs, consistent with the theoretical analysis result. Therefore, the stiffness evaluation indices and methods are rational.

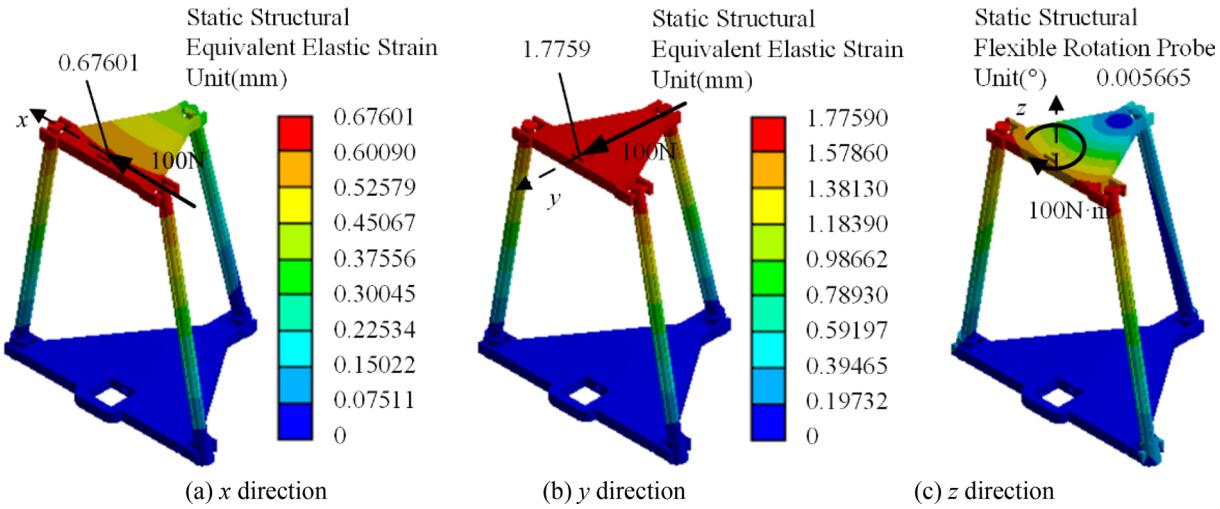

(a) *x* direction (b) *y* direction (c) *z* direction

Figure 19 Deformation of the 2UPU/SP PM in different directions

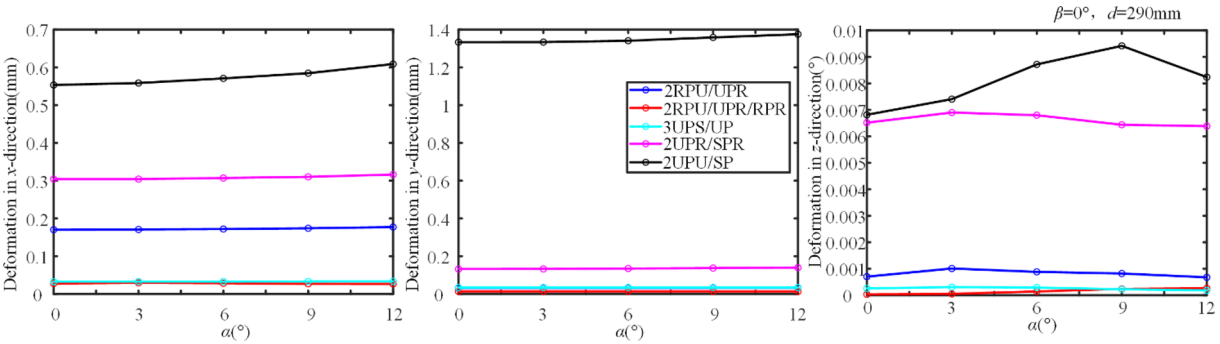

Figure 20 The maximum deformation in *x*, *y* and *z*-axis of five PMs with respect to variable *α*

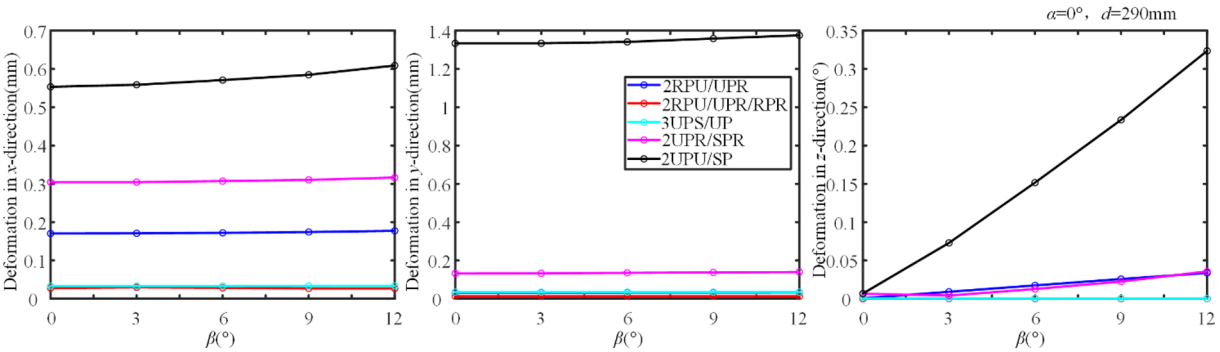

Figure 21 The maximum deformation in *x*, *y* and *z*-axis of five PMs with respect to variable *β*

7 Conclusions

To address the challenge of evaluating the configuration stiffness performance of PMs, new evaluation indices and a corresponding method are proposed. Utilizing these, the stiffness performances of five PMs are compared.

(1) Bending and torsional stiffness evaluation indices for PMs have been proposed, along with a method for assessing the PMs' configuration stiffness. Furthermore, the established model is applied to a real case study. Then various driving and structural

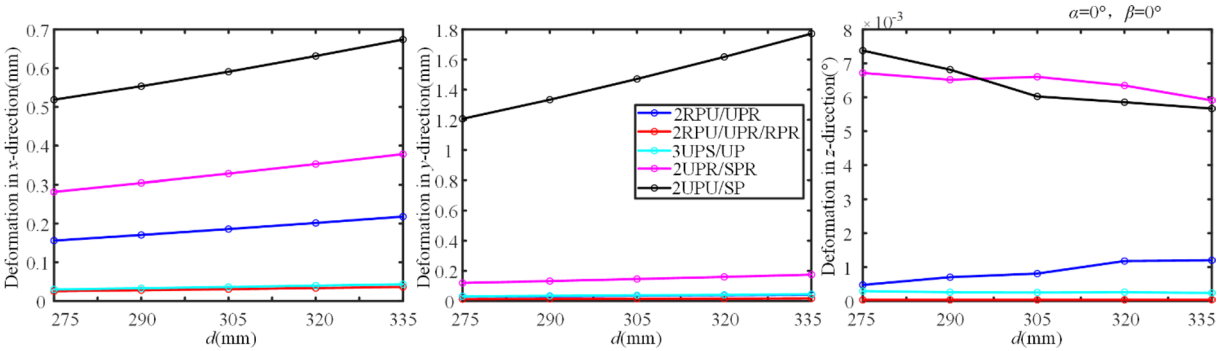

Figure 22 The maximum deformation in *x*, *y* and *z*-axis of five PMs with respect to variable *d*

stiffness of each branch affecting the configuration stiffness are evaluated, and their specific values are defined. Then, an external load is applied, and the bending and torsional deformation of each PM is calculated. The results obtained from these calculations are utilized to evaluate the parallel mechanism's bending and torsional stiffness performance.

(2) Based on simulations performed in ADAMS and ANSYS environments, a practical solution is proposed to solve the non-dynamic problem of the mechanism, including the prismatic joints. This approach introduces the concept of modal files containing multi-interface nodes. By discretizing the rigid areas within the flexible body, the dynamic behavior of the model is simulated, resulting in a rigid-flexible hybrid model for the over-constrained PM. This model enables continuous force simulation analysis of the over-constrained PM with P joints throughout the entire workspace.

(3) Based on the stiffness evaluation indices and methods, the configuration stiffness performance of the five 2R1T PMs is compared and analyzed. The 2RPU/UPR/RPR mechanism has relatively good bending and torsional stiffness preferred as the PM part of the five-axis hybrid machining robot. Additionally, the comparison results demonstrate that the stiffness of four-branch PMs is not necessarily greater than three-branch PMs.

The proposed stiffness evaluation method can also be applied to other PMs. In our future work, we will evaluate more PMs and select those with greater configuration stiffness.

Acknowledgements
Not applicable.

Author Contributions
XM was in charge of the whole data analysis; XM and ZX wrote the manuscript; YX and YZ directed the research and writing of the paper. All authors read and approved the final manuscript.

Funding
Supported by National Natural Science Foundation of China(Grant Nos. 51875495, U2037202), and Hebei Provincial Science and Technology Project (Grant No. 206Z1805G).

Data availability
The data that support the findings of this study are available from the corresponding author, [Xu Y D], upon reasonable request.

Declarations

Competing Interests
The authors declare no competing financial interests.

Received: 21 December 2022 Revised: 26 February 2024 Accepted: 17 May 2024
Published online: 08 July 2024

References

[1] K H Hunt. Structural kinematics of in-parallel-actuated robot arms. *ASME J. Mech. Trans. Automat. Des.*, 1983, 105: 705–712.
[2] N M Rao, K M Ra. Dimensional synthesis of a spatial 3-RPS parallel manipulator for a prescribed range of motion of spherical joints. *Mech. Mach. Theory*, 2009, 44(2): 477–486.
[3] Y M Li, Q S Xu. Kinematic analysis of a 3-PRS parallel manipulator. *Robot Cim.-Int. Manuf.*, 2007, 23(4): 395–408.
[4] X J Liu, L P Wang, F G Xie, et al. Design of a three-axis articulated tool head with parallel kinematics achieving desired motion/force transmission characteristics. *Journal of Manufacturing Science and Engineering-Transactions of the ASME*, 2010, 132(2): 021009.
[5] F Gao, J L Yang, Q J Ge. Type synthesis of parallel mechanisms having the second class G_F sets and two dimensional rotations. *Journal of Mechanisms and Robotics-Transactions of the ASME*, 2011, 3(1): 011003.

[6] C Fan, H Liu, Y Zhang. Type synthesis of 2T2R, 1T2R and 2R parallel mechanisms. *Mech. Mach. Theory*, 2013, 61: 184–190.

[7] D M Gan, J Dias, L D Seneviratne. Unified kinematics and optimal design of a 3rRPS metamorphic parallel mechanism with a reconfigurable revolute joint. *Mech. Mach. Theory*, 2016, 96 (2): 239–254.

[8] D M Gan, J S Dai, J Dias, et al. Unified kinematics and singularity analysis of a metamorphic parallel mechanism with bifurcated motion. *ASME J. Mech. Des.*, 2013, 5(3): 031004.

[9] J Wei, J S Dai. Reconfiguration-aimed and manifold-operation based type synthesis of metamorphic parallel mechanisms with motion between 1R2T and 2R1T. *Mechanism and Machine Theory*, 2019, 139: 66–80.

[10] R D Gregorio. Inverse position analysis, workspace determination and position synthesis of parallel manipulators with 3-RSR topology. *Robotica*, 2003, 21(6): 627–632.

[11] Y G Li, H T Liu, X M Zhao, et al. Design of a 3-dof PKM module for large structural component machining. *Mech. Mach. Theory*, 2010, 45(6): 941–954.

[12] T Sun, Y M Song. Dimensional synthesis of a 3-DOF parallel manipulator based on dimensionally homogeneous Jacobian matrix. *Sci. China Technol. Sc.*, 2010, 53(1): 168–174.

[13] G Pond, J A Carretero. Architecture optimization of three 3-PRS variants for parallel kinematic machining. *Robot, Cim. Int. Manuf.*, 2009, 25: 64–72.

[14] D Zhang, C M Gosselin. Kinetostatic analysis and design optimization of the Tricept machine tool family. *ASME J. Manuf. Sci. Eng.*, 2002, 124(3): 725–733.

[15] T Huang, M Li, X M Zhao, et al. Conceptual design and dimensional synthesis for a 3-DOF module of the TriVariant—a novel 5-DOF reconfigurable hybrid robot. *IEEE T Robot*, 2005, 21(3): 449–456.

[16] Z M Bi, Y Jin. Kinematic modeling of Exechon parallel kinematic machine. *Robot Cim.-Int. Manuf.*, 2011, 27(1): 186–193.

[17] Y Jin, Z M Bi, H T Liu, et al. Kinematic analysis and dimensional synthesis of Exechon parallel kinematic machine for large volume machining. *ASME J. Mech. Rob.*, 2015, 7(4): 041004.

[18] T Huang, C Dong, H Liu, et al. A simple and visually orientated approach for type synthesis of overconstrained 1T2R parallel mechanisms. *Robotica*, 2019, 37(7): 1161–1173.

[19] L M Xu, X X Chai, Q C Li, et al. Design and experimental investigation of a new 2R1T overconstrained parallel kinematic machine with actuation redundancy. *Journal of Mechanisms and Robotics*, 2019, 11(3): 031016.

[20] Y Song, P Han, P Wang. Type synthesis of 1T2R and 2R1T parallel mechanisms employing conformal geometric algebra. *Mech. Mach. Theory*, 2018, 121:475–486.

[21] Z M Chen, W A Cao, H F Ding, et al. Continuous motion of a novel 3-CRC symmetrical parallel mechanism. *Proceedings of the Institution of Mechanical Engineers Part C-Journal of Mechanical Engineering Science*, 2016, 230(3): 392–405.

[22] Y D Xu, S H Ni, B Wang, et al. Design and calibration experiment of serial–parallel hybrid rotary platform with three degrees of freedom. *Journal of Mechanical Engineering Science*, 2019, 233(5): 1807–1817.

[23] F G Xie, X J Liu, T M Li. Type synthesis and typical application of 1T2R-Type parallel robotic mechanisms. *Math. Probl. Eng.*, 2013: 1–12.

[24] G Gogu. *Fully-isotropic T1R2-type parallel robots with three degrees of freedom*. California: ASME international design engineering technical conferences & computers and information in engineering conference, 2005. https://doi.org/10.1115/DETC2005-84313.

[25] Q Jin, T L Yang. Synthesis and analysis of a group of 3-degree-of-freedom partially decoupled parallel manipulators. *Journal of Mechanism Desing*, 2004, 126(2): 301–306.

[26] T Sun, X Huo. Type synthesis of 1T2R parallel mechanisms with parasitic motions. *Mech. Mach. Theory*, 2018, 128: 412–428.

[27] Q C Li, J M Hervé. 1T2R parallel mechanisms without parasitic motion. *IEEE Transactions on Robotics*, 2010, 26(3): 401–410.

[28] Y D Xu, D S Zhang, J T Yao, et al. Type synthesis of the 2R1T parallel mechanism with two continuous rotational axes and study on the principle of its motion decoupling. *Mech. Mach. Theory*, 2017, 108: 27–40.

[29] Q C Li, J M Hervé. Type synthesis of 3-DOF RPR-equivalent parallel mechanisms. *IEEE Transactions on Robotics*, 2014, 30(6): 1333–1343.

[30] Q C Li, L M Xu, Q H Chen, et al. New family of RPR-equivalent parallel mechanisms: Design and application. *Chinese Journal of Mechanical Engineering*, 2017, 30(2): 217–221.

[31] X W Kong, C M Gosselin. Type synthesis of three-DOF UP-equivalent parallel manipulators using a virtual-chain approach. *Advances in Robot Kinemtics: Mechanisms and Motion*, 2006: 123.

[32] Y D Xu, Y Zhao, Y Yue, et al. Type synthesis of overconstrained 2R1T parallel mechanisms with the fewest kinematic joints based on the ultimate constraint wrenches. *Mechanism and Machine Theory*, 2020, 147: 103766.

[33] C Zhao, H W Guo, D Zhang, et al. Stiffness modeling of n(3RRIS) reconfigurable series-parallel manipulators by combining virtual joint method and matrix structural analysis. *Mechanism and Machine Theory*, 2020, 152: 103960.

[34] W A Cao, H F Ding, W G Zhu. Stiffness modeling of overconstrained parallel mechanisms under considering gravity and external payloads. *Mechanism and Machine Theory*, 2019, 135: 1–16.

[35] J Zhang, Y Q Zhao, Y Jin. Kinetostatic-model-based stiffness analysis of Exechon PKM. *Robotics and Computer-Integrated Manufacturing*, 2016, 37: 208–220.

[36] H B Tian, H W Ma, J Xia, et al. Stiffness analysis of a metamorphic parallel mechanism with three configurations. *Mechanism and Machine Theory*, 2019, 142: 103595.

[37] B C Bouzgarrou, J C Fauroux, G Gogu, et al. Rigidity analysis of T3R1 parallel robot with uncoupled kinematics.. *Proc. of the 35th International Symposium on Robotics*, Paris, France, 2004.

[38] G Piras, W L Cleghorn, J K Mills. Dynamic finite-element analysis of a planar high-speed, high-precision parallel manipulator with flexible links. *Mech. Mach. Theory*, 2005, 40(7): 849–862.

[39] T Huang, X Y Zhao, D J Whitehouse. Stiffness estimation of a tripod-based parallel kinematic machine. *IEEE Transaction on Robotics and Automation*, 2002, 18(1): 50–58.

[40] D Zhang, F F Xi, C M Mechefske, et al. Analysis of parallel kinematic machine with kinetostatic modeling method. *Robotics and Computer-Integrated Manufacturing*, 2004, 20(2): 151–165.

[41] F Majou, C Gosselin, P Wenger, et al. Parametric stiffness analysis of the Orthoglide. *Mechanism and Machine Theory*, 2007, 42(3): 296–311.

[42] A Pashkevich, D Chablat, P Wenger. Stiffness analysis of overconstrained parallel manipulators. *Mechanism and Machine Theory*, 2009, 44(5): 966–982.

[43] Y M Li, Q S Xu. Stiffness analysis for a 3-PUU parallel kinematic machine. *Mech. Mach. Theory*, 2008, 43(2): 186–200.

[44] T Huang, H T Liu, D G Chetwynd. Generalized Jacobian analysis of lower mobility manipulators. *Mech. Mach. Theory*, 2011, 46(6): 831–844.

[45] B Hu, Z Huang. Kinetostatic model of overconstrained lower mobility parallel manipulators. *Nonlinear Dynamics*, 2016, 86(1): 309–322.

[46] T Sun, B Lian, Y Song. Stiffness analysis of a 2-DOF overconstrained rpm with an articulated traveling platform. *Mech. Mach. Theory*, 2016, 96:165–178.

[47] Y D Xu, W L Liu, J T Yao, et al. A method for force analysis of the overconstrained lower mobility parallel mechanism. *Mechanism and Machine Theory*, 2015, 88: 31–48.

[48] C Yang, Q C Li, Q H Chen, et al. Elastostatic stiffness modeling of overconstrained parallel manipulators. *Mechanism and Machine Theory*, 2018, 122: 58–74.

[49] T Sun, H Wu, B B Lian, et al. Stiffness modeling, analysis and evaluation of a 5 degree of freedom hybrid manipulator for friction stir welding. *Proceedings of the Institution of Mechanical Engineers*, 2017, 231(23): 4441–4456.

[50] Q Xu, Y Li. An investigation on mobility and stiffness of a 3-DOF translational parallel manipulator via screw theory. *Robotics and Computer-Integrated Manufacturing*, 2008, 24: 402–414.

[51] Rezaei, A Akbarzadeh, M R Akbarzadeh-T. An investigation on stiffness of a 3-PSP spatial parallel mechanism with flexible moving platform using invariant form. *Mechanism and Machine Theory*, 2012, 51: 195–216,

[52] D Wang, R Fan, W Y Chen. Stiffness analysis of a hexaglide parallel loading mechanism. *Mechanism and Machine Theory*, 2013, 70: 454–473,

[53] B Hu, Z Huang. Kinetostatic model of overconstrained lower mobility parallel manipulators. *Nonlinear Dynamics*, 2016, 86: 309–322.

[54] C Yang, Q Li, Q Chen, et al. Elastostatic stiffness modeling of overconstrained parallel manipulators. *Mechanism and Machine Theory*, 2018, 122: 58–74.

[55] J Ding, C Wang, H Wu. Accuracy analysis of redundantly actuated and overconstrained parallel mechanisms with actuation errors. *Journal of Mechanisms and Robotics*, 2018, 10(6): 061010.
[56] W A Cao, H Ding. A method for stiffness modeling of 3R2T overconstrained parallel robotic mechanisms based on screw theory andstrain energy. *Precision Engineering*, 2018, 51: 10–29.
[57] W A Cao, H Ding, D Yang. A method for compliance modeling of five degree-of-freedom overconstrained parallel robotic mecha-nisms with 3T2R output motion. *Journal of Mechanisms and Robotics*, 2017, 9: 011011.
[58] W A Cao, H Ding, W Zhu. Stiffness modeling of overconstrained parallel mechanisms under considering gravity and externalpayloads. *Mechanism and Machine Theory*, 2019, 135: 1–16.
[59] A Klimchik, A Pashkevich, D Chablat. *Stiffness modeling of navaro ii transmission system*. Berlin: IFAC PapersOnLine, 2019, 52(13): 701–706.
[60] A Klimchik, A Pashkevich, D Chablat. Fundamentals of manipulator stiffness modeling using matrix structural analysis. *Mechanism and Machine Theory*, 2019, 133: 365–394.
[61] Yang, W Ye, Q C Li. Review of the performance optimization of parallel manipulators. *Mechanism and Machine Theory*, 2022, 170: 104725.
[62] Y Li, Q Xu. Stiffness analysis for a 3-PUU parallel kinematic machine. *Mech. Mach. Theory.*, 2007, 43: 186–200.
[63] G Carbone, M Ceccarelli. Comparison of indices for stiffness performance evaluation. *Frontiers of Mechanical Engineering*, 2010, 5(3): 270–278. DOI:https://doi.org/10.1007/s11465-010-0023-z.
[64] D Zhang, Z Gao. Optimization design of a spatial *six-degree-of-freedom parallel manipulator based on genetic algorithms and neural networks*. Proceedings of the ASME International Design Engineering Technical Conferences and Computers and Information in Engineering Conference, 2009: 767–775.
[65] E Courteille, D Deblaise, P Maurine. Design optimization of a delta-like parallel robot through global stiffness performance evaluation. *2009 IEEE-RSJ International Conference on Intelligent Robots and Systems*, St. Louis, 2009: 5159–5166. https://doi.org/10.1109/IROS.2009.5353906.
[66] Y Jin, Z M Bi, H T Liu, et al. Kinematic analysis and dimensional synthesis of Exechon parallel kinematic machine for large volume machining. *Journal of Mechanisms and Robotics*, 2015, 7(4): 041004.
[67] W L Liu, Y D Xu, L L Chen, et al. Solving the force problem of passive overconstrained rigid-flexible mixed parallel mechanisms based on the generalized inverse of weighted moore-penrose. *China Mechanical Engineering*, 2016, 52(23): 84–93.(in Chinese)
[68] K E Neumann. Next generation tricept—a true revolution in parallel kinematics. *Parallel Kinematic Machines in Research and Practice*, 2004, 24: 591–594.
[69] Y D Xu, F Yang, Z H Xu, et al. TriRhino: A five-degrees-of-freedom of hybrid serial–parallel manipulator with all rotating axes being continuous: Stiffness analysis and experiments. *Journal of Mechanisms and Robotics*, 2021,13(2): 025002.
[70] D S Zhang, Y D Xu, J T Yao, et al. Design of a novel 5-DOF hybrid serial-parallel manipulator and theoretical analysis of its parallel part. *Robotics and Computer Integrated Manufacturing*, 2018, 53: 228–239.
[71] W L Liu, Y D Xu, J T Yao, et al. The weighted Moore-Penrose generalized inverse and the force analysis of overconstrained parallel mechanisms. *Multibody System Dynamics*, 2017, 39(4): 363–383.
[72] W L Liu, Y D Xu, J T Yao, et al. Methods for force analysis of over-constrained parallel mechanisms: a review. *Chinese Journal of Mechanical Engineering*, 2017, 30(6): 1460–1472.

Xuejian Ma born in 1997, is currently a PhD at the *School of Mechanical Engineering Yanshan University, China*. He received his bachelor degree from *Yanshan University, China,* in 2016. His research interests include parallel mechanisms and hybrid robots.

Zhenghe Xu born in 1977, received his master degree from *Yanshan University, China*, in 2020.

Yundou Xu born in 1985, is currently a professor at the *School of Mechanical Engineering, Yanshan University, China*. His research interests include parallel structure theory and its applications.

Yu Wang is currently a PhD at the *School of Mechanical Engineering*, *Yanshan University, China*. His research interests include parallel mechanisms and hybrid robots.

Jiantao Yao born in 1980, is currently a professor at the *School of Mechanical Engineering, Yanshan University, China*. His research interests include Special robots, soft robots, and six-dimensional force sensors.

Yongsheng Zhao born in 1962, is currently a professor at the *School of Mechanical Engineering, Yanshan University, China*. His research interests include Robotics technology, sensor technology, and advanced manufacturing technology.